Constraining the North Atlantic circulation between 4.5°S and 39.5°N with transient tracer observations

Xingwen Li

MIT/WHOI Joint Program in Physical Oceanography, Massachusetts Institute of Technology, Cambridge, Massachusetts, USA

Carl Wunsch

Department of Earth, Atmospheric and Planetary Sciences, Massachusetts Institute of Technology, Cambridge, Massachusetts, USA

Received 27 December 2002; revised 17 July 2003; accepted 28 July 2003; published 10 October 2003.

[1] A 1° horizontal resolution North Atlantic general circulation model (GCM) in the latitude band 4.5°S to 39.5°N is compared to, and then combined with, chlorofluorocarbon and tritium transient tracer data. The method of Lagrange multipliers (adjoint) is used. Tracer distribution within the model ocean interior is primarily sensitive to the flux through the open northern boundary. This flux is determined by the estimation method and is found to deviate from the initial estimate significantly for all tracers. An attempt to carry the model domain to 78.5°N showed the GCM inadequacy, believed to be primarily a problem of spatial resolution, to compute the convective injection of tracer into the deep ocean. Any such errors persist throughout the tracer integration and corrupt all further tracer concentrations. In general, and consistent with earlier much simpler computations, uncertainties in surface and northern boundary conditions dominate the computed tracer concentrations. The final results here are improved estimates of the three-dimensional time histories of the tritium and CFCs and their boundary conditions over the model domain, with very little information available to constrain the GCM itself in the latitude band. *INDEX TERMS:* 4532 Oceanography: Physical: General circulation; 4842 Oceanography: Biological and Chemical: Modeling; 4255 Oceanography: General: Numerical modeling; 4271 Oceanography: General: Physical and chemical properties of seawater; *KEYWORDS:* transient tracer, state estimation, adjoint model

Citation: Li, X., and C. Wunsch, Constraining the North Atlantic circulation between 4.5°S and 39.5°N with transient tracer observations, *J. Geophys. Res.*, *108*(C10), 3318, doi:10.1029/2002JC001765, 2003.

1. Introduction

[2] As a result of the World Ocean Circulation Experiment (WOCE) and earlier expeditions, transient tracer data in the ocean are now comparatively common. This type of data has been used for a number of different oceanographic purposes. One major application has been the production of concentration charts from which are inferred large-scale ocean circulation pathways [e.g., *Schlosser et al.*, 1991; *Doney and Bullister*, 1992; *Smethie et al.*, 2000]. A number of studies exist in which these data have been used to infer mixing rates [e.g., *Jenkins*, 1991; *Matear and Wong*, 1997; *Haine et al.*, 1998]. In other recent studies, transient tracer inventories have been used to estimate the formation rates of Antarctic Bottom Water (AABW) [*Orsi et al.*, 1999], the North Atlantic Deep Water (NADW) [*Smethie and Fine*, 2001], Labrador Sea Water (LSW) [*Rhein et al.*, 2002], and others. Transient tracer observations have also been used as tests of general circulation models (GCMs) [e.g., *Craig et al.*, 1998; *Heinze et al.*, 1998; *England and Maier-Reimer*, 2001]. In contrast however, only a comparatively small theoretical literature exists [e.g., *Wunsch*, 1988, 2002; *Waugh et al.*, 2003; *Haine and Hall*, 2002; *Deleersnijder et al.*, 2001] concerning the use of the tracers. Much of this literature is directed at theoretical tracers computable in models and useful in model diagnostics rather than at the use of realistic observations.

[3] Estimates of oceanic parameters have long been made from more conventional oceanographic data of all kinds [e.g., *Wunsch*, 1996, hereinafter W96; *Ganachaud and Wunsch*, 2003]. In this paper, we attempt to understand the extent to which transient tracers carry unique information, relative to other data sources, about the large-scale ocean circulation, and to produce model states in accord with that information. The second goal is a form of state estimation (assimilation), in which one simultaneously formalizes the testing of models against the tracer data and forces the model, as far as is physically and statistically possible, to consistency with the data.

0148-0227/03/2002JC001765$09.00

[4] As has been long recognized, a major issue in using transient tracer data with models lies with the difficulty of reconstruction of the boundary conditions through time from real observations. In contrast with quasi-steady fields such as oxygen, data from various years cannot be combined; each year is unique, and there is a similar reconstruction problem with the time-varying interior distributions. Unobserved boundary data cannot be reconstructed by direct observation after the fact.

[5] One of the major transient tracers, tritium (^{3}H), entered the ocean primarily in the 1960s when observations were sparse [*Dreisigacker and Roether*, 1978]. For ^{3}H, chlorofluorocarbons (CFCs) and radiocarbon (^{14}C) estimates of the surface fluxes also rest on limited knowledge of the complex air-sea gas exchange process. The relationship between the gas transfer velocity and wind speed is not well understood [*Wanninkhof*, 1992]; the effects of boundary layer stability, turbulence, and bubbles in the air-sea tracer exchange are still uncertain. Inevitably, large uncertainties exist in the estimates of the transient tracer input functions. A focus of this present study is learning to interpret transient tracer distributions with uncertain input histories. Another family of transient tracers exists, that from regional purposeful releases [*Ledwell et al.*, 1993, etc.]; these data are not considered here.

[6] Consider any passive tracer C, whose concentration is governed by an advection/diffusion equation of form,

$$\frac{\partial C}{\partial t} + \mathbf{u} \cdot \nabla C - \nabla \cdot (\mathbf{K} \nabla C) = -\lambda C + S, \qquad (1)$$

where S represents sinks/sources, λ is a decay constant, $\mathbf{u}$ is velocity, and $\mathbf{K}$ is a mixing tensor, all of which are normally assumed known in solving the "forward" or "direct" problem. This problem is the conventional one, whereby given $C(\mathbf{r}, t = 0) = C_0(\mathbf{r})$, the initial conditions, and $C(\mathbf{r} = \mathbf{r}_B, t) = C_B(t)$, the concentration boundary conditions, one calculates $C(\mathbf{r}, t)$, where $\mathbf{r}$ is the three-dimensional space coordinate, and $\mathbf{r}_B$ defines the boundary positions. (Flux or mixed boundary conditions are equally suitable.) Any uncertainty in the values of $\mathbf{u}$, $\mathbf{K}$, S, C_0, C_B propagates through the system, introducing errors and uncertainties in $C(\mathbf{r}, t)$. The inverse, or state estimation problem, was studied in idealized circumstances by *Wunsch* [1988]. There, one has some incomplete knowledge of $C(\mathbf{r}_i, t_i)$,$C_B(t_j)$,$C_0(\mathbf{r}_k)$, and attempts to make inferences about $\mathbf{u}$, $\mathbf{K}$, S. An infinite number of possible problems can be posed involving differing assumptions about what is known and how well it is known. One rapidly concludes that sparsity of data defining $C(\mathbf{r}_i, t_i)$, $C_B(t_j)$, $C_0(\mathbf{r}_k)$ looms as a large problem, with the chemical analytical uncertainties of comparatively minor concern.

[7] Despite the paucity of data, it is not widely understood that even a few data points can sometimes provide stringent tests of an oceanic model. Consider a hypothetical case for tritium, in which the only knowledge was that there was no ambient tritium concentration in 1940, and that the surface tritium concentration over the succeeding years could be only very crudely bounded as $C_B(t) < B$ and that tritium was measured at a single point $\mathbf{r}_1$, at some time t_1: $C(\mathbf{r}_1, t_1) \pm \Delta C_1$. If, in running the model, one finds the computed value, C_m, produces $|C_m(\mathbf{r}_1, t_1) - C(\mathbf{r}_1, t_1)| \gg \Delta C_1$, one might sensibly conclude there was something drastically wrong with the model, and hence reject it (as we will do below). The inverse (state estimation) problem takes another step: Are there adjustable elements of the model, which could be changed within acceptable limits so that $|C_m(\mathbf{r}_1, t_1) - C(\mathbf{r}_1, t_1)| = O(\Delta C_1)$? If the answer is "yes", one might regard the adjusted model as being better than the one used originally. It is possible however, that no such adjustment can be made, even with one data point, and the model rejected as inadequate. In the former situation, however, one cannot claim that the model has been "validated", only that it is consistent with the observations.

[8] Systematic methods exist for (1) comparing models with data, of almost any type, and then (2) finding the smallest perturbations that might render model and data consistent. In practice, such state estimation methods almost always reduce to least-squares fitting of a model to observations, albeit, sometimes this underlying simplicity is thoroughly disguised by the algorithms necessary to handle large volumes of numbers.

[9] A considerable literature exists on state estimation using observations such as altimetry, XBTs, and traditional hydrographic data both in steady (e.g., W96) and time-varying ocean models [*Stammer et al.*, 2002, 2003]. The assimilation of these conventional observations is able to correct for many features that are often poorly simulated in traditional numerical simulations, such as the strengths of the Gulf Stream and its extension, the Azores Current and the anticyclonic circulation associated with the Labrador Sea. The time-mean transports of heat and freshwater from the constrained model solutions are converging with the independent steady-flow estimates from box inversions over most parts of the world ocean.

[10] Comparatively few examples exist of the use of transient tracers. *Mémery and Wunsch* [1990] (hereinafter MW), using a geostrophic box model and a Green function approach, showed that uncertainty in the tritium boundary conditions and sparse data coverage greatly weakened the ability of tritium to constrain their model. *Gray and Haine* [2001] (hereinafter GH) combined a North Atlantic ocean general circulation model (OGCM) with chlorofluorocarbon observations, also using the Green function method. In their work, the model-data misfit was minimized by the improved estimates of gas transfer rates at the air-sea interface in the high latitudes. They concluded that after the optimization of the surface fluxes, the model and data were marginally consistent. Here we further explore the capability of present transient tracer observations to constrain ocean circulation properties.

2. Model Description

[11] The model used here is an "off-line" version [*Dutkiewicz et al.*, 2001] of the MIT GCM [*Marshall et al.*, 1997a, 1997b] together with its adjoint (see W96 or *Marotzke et al.* [1999] for discussion of adjoint models). That is, equation (1) is used with the three-dimensional velocity and mixing field obtained from the full GCM in forward mode, initialized with the Levitus hydrographic climatology and driven by climatological winds for a spin-up period of 40 years. The full GCM is then driven by 12-hourly analyzed winds and surface fluxes of heat and

fresh water (obtained from the National Meteorological Center reanalysis [*Kalnay et al.*, 1996]) from January 1987 to January 1995. The three-dimensional flow fields are the monthly means from 1987 to 1995. In the off-line model, the Gent et al. [*Gent and McWilliams*, 1990; *Gent et al.*, 1995] mixing scheme is used to parameterize the eddy-induced tracer transport. Deep mixed layers are formed by increasing the vertical diffusivity. The convective mixing is treated implicitly in a scheme producing a tracer distribution that is a continuous function of the enhanced mixing rates.

[12] From here on, unless specifically stated, the "model" refers to this off-line code. The model domain extends from 99.5°W to 21.5°E, 4.5°S to 39.5°N at 1° × 1° horizontal resolution. There are 21 vertical levels in the model with non-uniform resolution ranging from 25 m at the surface to 500 m near the ocean bottom. Realistic topography is employed. Parts of the northern, eastern, and southern boundaries are open. Non-zero tracer fluxes are allowed at these open boundaries.

[13] By focusing on the off-line model, we greatly restrict and simplify the state estimation problem. If the off-line model is unable to be brought into consistency with the observations, one would naturally turn to the problem of adjusting the underlying GCM, as did *Stammer et al.* [2002], a problem requiring much more intensive computation. Apart from some difficulties at high northern latitudes discussed below, in the present case, the off-line model proves adequate.

3. Adjoint Method

[14] The adjoint method is described by W96, and the particular form used here is described by *Marotzke et al.* [1999]. Some variables, $\mathbf{u}(t)$, are identified as "controls", subject to modification so as to bring the model state, $\mathbf{x}(t)$, the tracer concentrations, into consistency with the observations. Here the control variables include both initial and boundary conditions, and in some cases, interior parameters such as mixing coefficients. An objective function measures the model/data misfit, in the form,

$$J(\mathbf{x},\mathbf{u}) = \sum_t \Big\{ [\mathbf{y}(t) - \mathbf{E}(t)\mathbf{x}(t)]^T \mathbf{R}(t)^{-1} [\mathbf{y}(t) - \mathbf{E}(t)\mathbf{x}(t)] + \mathbf{u}(t)^T \mathbf{Q}(t)^{-1} \mathbf{u}(t) \Big\}, \quad (2)$$

using the notation of W96, where $\mathbf{y}(t)$ is the vector of observations at time t, and $\mathbf{E}(t)$ is here a zero matrix except at those locations where a measurement of $\mathbf{x}(t)$ is available, where it has a unit element. $\mathbf{R}(t)$ is the covariance matrix of the errors in $\mathbf{y}(t)$ and $\mathbf{Q}(t)$ is the covariance matrix of the controls. Both observation noise and controls are assumed to have zero expected value. The optimization problem requires minimizing J through changes in $\mathbf{u}(t)$, and consequently $\mathbf{x}(t)$, so that the misfits, $\mathbf{y}(t) - \mathbf{E}(t)\mathbf{x}(t)$, are acceptably small in a statistical sense (see W96). At all times, the state vector and the control variables must continue to satisfy the discrete analogue of equation (1); that is, we are solving a constrained optimization problem.

[15] The method used is that of Lagrange multipliers, sometimes known as the "adjoint method" because it uses the adjoint to equation (1) as an estimate of the derivatives of J in a descent procedure. The adjoint model is obtained here from the forward code in a semi-automatic way using the Tangent Linear and Adjoint Model Compiler (TAMC) [*Giering and Kaminski*, 1998; *Marotzke et al.*, 1999]. A quasi-Newton method is used for searching the descent direction. This approach uses the change of the gradient to obtain information on the local Hessian of the cost function. It computes an approximation to the curvature of the function without actually forming the Hessian matrix. The method converges very rapidly, but as configured, requires a large amount of memory.

[16] Because the adjoint model is derived from the derivatives of J with respect to model parameters and data, it represents the system sensitivity to perturbations in parameters and data. As such, the adjoint model carries a great deal of information about the forward model. For reasons of space however, the results of an analysis of the Lagrange multipliers (the "adjoint solution") are deferred to a companion paper (X. Li and C. Wunsch, An adjoint sensitivity study of chlorofluorocarbons in the North Atlantic, submitted to *Journal of Geophysical Research*, 2003) (hereinafter referred to as Li and Wunsch, submitted manuscript, 2003).

4. Data

[17] CFCs, which are entirely artificial, underwent atmospheric increases continuously from the 1930s to the early 1990s (Figure 1), when the Montreal Protocol led to their control. CFCs enter the ocean through air-sea gas exchange at the sea surface and the ocean shows, qualitatively, a similar strong increase over this same period.

[18] Tritium, the unstable isotope of hydrogen, ^{3}H, is found in the ocean as tritiated water (HTO). Tritium entered the ocean through direct precipitation, water vapor exchange between the atmosphere and ocean, and river outflows [e.g., *Weiss and Roether*, 1980; *Doney et al.*, 1993], primarily in the early 1960s. Because of the short decay time (half-life 12.43 years), the natural background of ^{3}H is negligible for present purposes.

[19] Tritium is measured in "tritium units", TU, in the HTO to H_2O ratio of 10^{-18}. TU81 refers to the tritium concentration that is decay-corrected to January 1, 1981 [e.g., *Östlund and Rooth*, 1990]. The decay-product of tritium is stable helium-3 (^{3}He), which also occurs naturally in the ocean from mantle outgassing.

[20] About 20,000 CFC-11/CFC-12 and 5000 tritium samples are available for this present study during 1972–1999, in the North Atlantic between 4.5°S and 39.5°N (Figure 2). Details of the data used are also given by *Li* [2003] and in Tables 1 and 2. The CFC-11 and CFC-12 data in the North Atlantic from WOCE and pre-WOCE have been collated. The tritium data are nearly the same as used by *Khatiwala et al.* [2001].

5. Boundary Conditions of the Transient Tracers

[21] CFC fluxes through the ocean surface are computed using a piston-velocity, K_w, flux parameterization,

$$F = K_w(C_e - C_s), \quad (3)$$

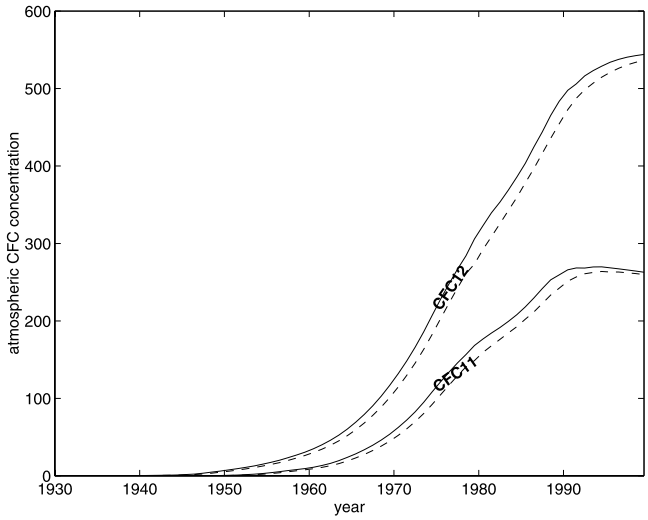

Figure 1. Estimates of atmospheric CFC-11 and CFC-12 concentrations (parts per trillion) as a function of time and hemisphere, following *Walker et al.* [2000]. Values in the Southern Hemisphere are dashed.

where C_s is the modeled sea surface tracer concentration. The oceanic surface equilibrium, C_e, of CFC-11 or -12, depends on the surface temperature and salinity [*Warner and Weiss*, 1985]. As the solubility properties and the atmospheric concentrations of CFCs are well known, the uncertainties of the CFC fluxes are mainly due to the uncertainties in K_w, and the multiplicative nature of K_w will absorb the remaining errors in C_e, C_s.

[22] A monthly climatology of K_w, taken from Ocean Carbon-Cycle Model Intercomparison Project (OCMIP) [http://www.ipsl.jussieu.fr/OCMIP], is computed from the equation adapted from *Wanninkhof* [1992],

$$K_w = (1 - F_i)\left[a\left(u_w^2 + \sigma_w^2\right)\right](Sc/660)^{-1/2}. \quad (4)$$

Here F_i is the fraction of the local sea surface covered with ice, and which varies from 0 to 1; u_w is the monthly climatological surface wind speed; σ_w^2 is the variance of u_w; a is a constant; Sc is the dimensionless Schmidt number calculated as $Sc = a_1 + a_2\theta + a_3\theta^3 + a_4\theta^4$, with θ the sea surface temperature in Celsius. More details can be found at the above-referenced web page. Values of a_1 to a_4 in the Schmidt number formula are from *Zheng et al.* [1998, equations (9) and (10)] .

[23] For tritium, a surface concentration boundary condition is used. Following the results of *Dreisigacker and Roether* [1978] and *Doney et al.* [1992], the tritium surface boundary concentration is supposed to be separable in time and space. The time history for years 1950–1986 is from *Doney et al.* [1993] (Figure 3). After 1986, the tritium surface concentration is extended by assuming an exponential (radioactive) decay. The spatial distribution of surface tritium, in Figure 4, is based on work by *Dreisigacker and Roether* [1978] and *Doney et al.* [1992]. The absolute value of tritium surface concentration is obtained by multiplying the temporal part with the corresponding spatial part.

[24] At the lateral boundaries, initial estimated concentrations of CFC-11, CFC-12 and tritium are obtained from an unconstrained model run over the North Atlantic between 4.5°S and 78.5°N [*Li*, 2003]. CFCs and tritium are simulated from a zero background at the beginning of 1940.

6. Data and Model Errors

[25] The data error covariance matrix, **R**, in equation (2) determines the extent to which the model and data can be expected to agree, something that depends on the accuracies of both data and model. If model-data differences lie within the uncertainties of both, the model is consistent with the data, and no further work is justified. In practice, these errors, particularly for the model, are poorly known.

[26] The tracer distribution along a section is regarded as nearly synoptic and is represented as occurring at time t_0,

$$y_i(t_0) = C(\mathbf{r}_i, t_0) + n_i(t_0), \quad (5)$$

where $n_i(t_0)$ includes not only any analytical noise, but also any deviation owing to, for example, eddy variability from a temporal average over a finite time interval (e.g., if $C(\mathbf{r}_i,t_0)$ is intended to be an annual mean). Model error can be included in the apparent data error, simply by defining the latter to include any component of the measurement not representable by the model (e.g., internal wave or eddy-variability), and that is the point of view we adopt.

[27] Measurement errors include those from both analytical and navigation problems. The analytical precisions of CFC-11, CFC-12, and tritium are about 0.005 pmol/kg, 0.005 pmol/kg, and 0.02 TU, respectively. Navigation error is minor, compared to the subgrid scale (about 100 km in our model) variability that the model cannot resolve.

[28] Error due to variability includes both temporal and spatial components. Temporal variability over a cruise duration (around a month) is estimated in part with the help of the GCM. The spatial part has several sources including small-scale turbulence, internal waves, and mesoscale

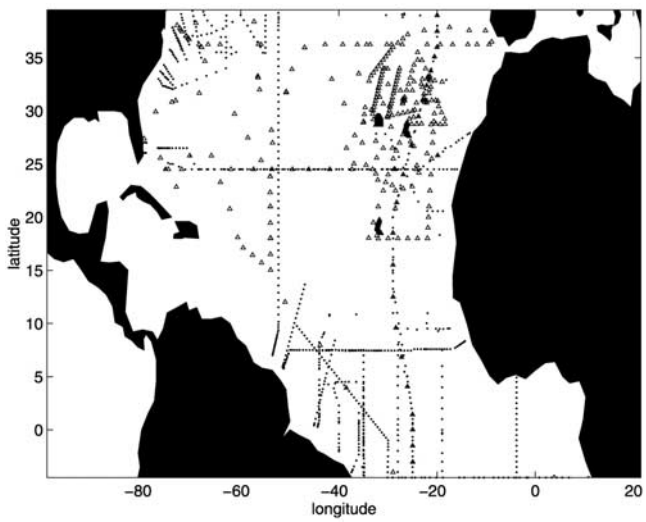

Figure 2. Map of tracer stations used in the assimilation process. Dots represent CFC-11/CFC-12 stations; triangles represent tritium stations.

Table 1. CFC-11 and CFC-12 Data Sources

Cruise	Reference
WOCE section A01EW, A01W, A05, A06, A07, A15, A17, A22, A24, AR04A-E, AR07EH, AR07WC, AR07WD, AR12B, AR13A-D	WOCE Hydrographic Program (2000)
WOCE section AR21, AR01, Transient Tracer in the Ocean expedition	John Bullister, personal communication, 2000
Endeavor214, 223, Knorr 134, Oceanus134, WOCE section A20	Bill Smethie, personal communication, 2000
Charles Darwin62	Martin Gould, personal communication, 2000
Oceanus202	*Doney and Bullister* [1992]
WOCE section A01E, A02A, METEOR393	Wolfgang Roether, personal communication, 2000

eddies. The spatial variances of the modeled tracer distributions are calculated as a function of depth and time, with the variance contributed by the subgrid scale taken to be 1/9 [e.g., *Stammer et al.*, 2002; *Haine and Gray*, 2001] of the variance obtained from the model. *Haine and Gray* [2001] showed that it was the subgrid spatial variability that dominated the error budget, and which is well over an order of magnitude greater than the temporal and instrumental errors, consistent with our result.

[29] The first step in using a model with data, before any attempt at state estimation is made, must always be a quantitative comparison of the forward model estimates with the data. In the original formulation, the model extended to 78.5°N, and *Li* [2003] describes a comparison of the forward model with both tritium and CFC data. Model/data differences are dominated by a strong tendency for the model to convect much too vigorously in the Labrador Sea and surrounding areas of the subpolar gyre. The major error then is that the model carries C in much too large quantities to great depths; consequently, all subsequent time history of C differs from what is observed, at least in large part owing to this problem alone.

[30] When a model produces obvious discrepancies with observations, the preferred next step is to modify the model to be more realistic before any state estimation occurs. In the present case, much of the difficulty with high-latitude convection is believed tied to the limited model resolution [e.g., *Marshall and Schott*, 1999], both vertical and horizontal and the conceptually simplest solution to the problem renders it computationally too burdensome at the present

Table 2. Tritium and Helium Data Sources Except That From *Khatiwala et al.* [2001]

Cruise	Reference
Oceanus202	Scott Doney, personal communication, 2000
WOCE section A01E, A02A, METEOR393	Wolfgang Roether, personal communication, 2000
GEOSECS, Transient Tracer in the Ocean, North Atlantic Tracer Sections expedition	H.G. Östlund, personal communication, 2000
Pilot Subduction study, 1991–1993 Subduction study	WHOI Helium Isotope Lab

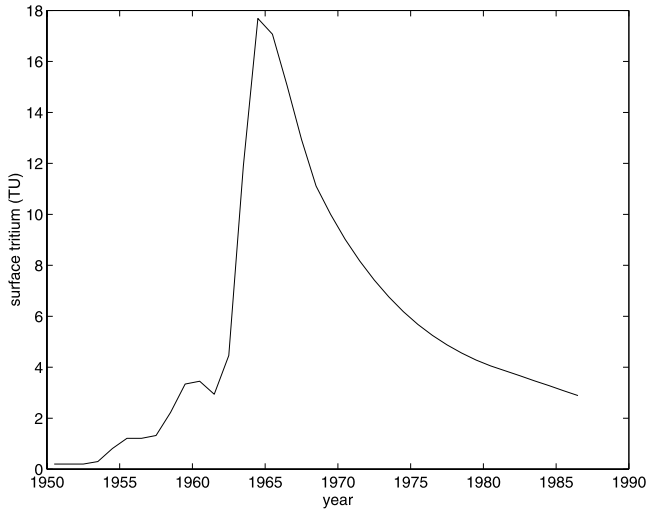

Figure 3. Temporal distribution of tritium concentration in the North Atlantic surface water, following *Dreisigacker and Roether* [1978] and *Doney et al.* [1993].

time. As an alternative, to permit further exploration of the model and data, the simple expedient of reducing the model domain to the region south of 39.5°N was used. This northern boundary is an open one, with the tracer concentration there becoming part of the control vector whose values are to be adjusted. (Experiments, not described here, were carried out using the model in the full domain, and permitting, for example, the piston velocities to be reduced in the convective regions so as to render the interior tracer distributions more realistic. The resulting piston velocity values are unphysical and the model in that area is rejected as inadequate.)

[31] Figure 5 shows the vertical profiles of the data errors, dominated by the unresolved subgrid variability, in 4.5°S–39.5°N, 99.5°W–21.5°E, 1990. Uncertainties are large near

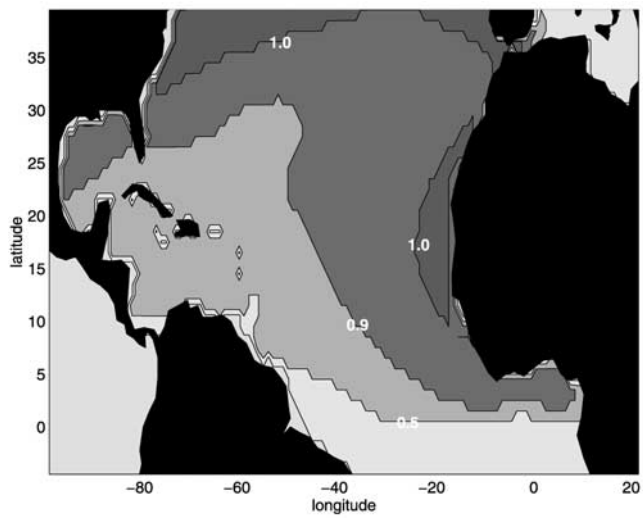

Figure 4. Estimated spatial coefficient of tritium concentration in the North Atlantic surface water; to obtain absolute tritium concentration, value in this figure has to be multiplied by the temporal distribution in Figure 3.

the surface, because the subgrid scale variability (much of it mesoscale eddies) there are large, and they decrease with depth. Substantial uncertainties exist above 4500 m, due to the variability of the upper and intermediate water masses, and the North Atlantic Deep Water (NADW). Below 4500 m depth, the uncertainties are very small. This inference is consistent with the fact that both transient tracer concentrations and their variability in this part of the ocean are small. Since the CFC-11 content in the ocean in 1990 is large, the amplitude of its variability is relatively large and the uncertainty prescribed for CFC-11 concentration in 1990 is larger than that for CFC-12 and tritium.

[32] In our model-data comparison, the data are binned meridionally, zonally, and vertically onto the model grid cells. A cell average is calculated if more than one sample is available within a cell. Monthly averages of data and model outputs are compared.

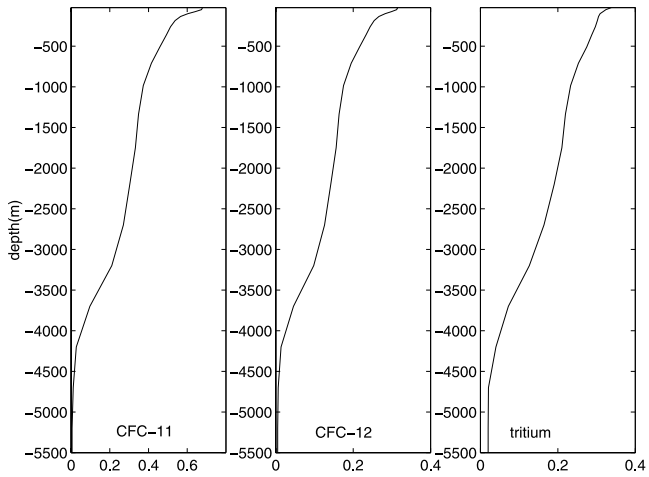

Figure 5. Uncertainty profiles prescribed for different tracers in area 4.5°S–39.5°N, 99.5°W–21.5°E, 1990. Units of CFC and tritium are pmol/kg and TU, respectively.

7. Optimization of the CFC Boundary Conditions

[33] As discussed by MW, a central difficulty in using transient tracers as constraints on ocean models lies with the uncertainty of the boundary conditions. For tracers that are at least nominally steady (up to comparatively small interannual and higher frequency variability), one can reconstruct the boundary conditions by combining observations from multiple cruises over multiple years or even decades, with averaging reducing the errors. For the transient tracers used here, such a pooling of decadal data sets is impossible; in some cases, for example, the early to mid-1960s for tritium, the year to year variation in surface fluxes or concentrations is a major part of the transient signal. The rather sparse, sporadic coverage in any particular year over the CFC or ^{3}H transient means that large uncertainties remain in the surface/lateral boundary condition values, and these uncertainties have a direct, zero-order influence on the ability to use the data as constraints. (Note, too, that strong transients in surface conditions greatly exacerbate the problem of modeling high-latitude convection already described: If the model fails to convect in the right year, in the right location, but is otherwise extremely accurate, the injected tracer will be computed incorrectly, with subsequent errors ever-after.)

[34] Following MW, therefore, we begin by determining whether observed model data differences, $\mathbf{y}(t) - \mathbf{E}(t)\,\mathbf{x}(t)$, beyond the estimated limits of error, can be removed by the simple expedient of modifying the boundary conditions within acceptable limits. If the answer is affirmative, the tracer data can provide no further information about the interior model physics.

[35] Consider first the CFCs. The control vector comprises the yearly-varying open-boundary concentrations, the initial tracer state, and monthly mean climatological piston velocities. An integration period over the years 1981–1999, within which all CFC data available fall, is chosen to minimize the number of control variables representing the open boundary conditions. A fractional uncertainty of 30% (following GH) is taken for the piston velocity estimate in this study. Northern, southern, and a part of the eastern boundaries are open. Tracer concentrations there are part of the control vector whose values are to be adjusted. Initially, the relative uncertainties of open boundary and interior tracer concentrations (both taken from the unconstrained forward model run) are assumed to be 100%. A lower bound on the error of 0.005 pmol/kg CFC concentrations is enforced everywhere on the basis that the systematic errors are at least this large.

[36] For want of any information about the spatial structure of the uncertainty, a diagonal weight matrix, **R**, is used and

$$J = \sum_t \left\{ \sum_i \frac{(y_i(t) - x_i(t))^2}{R_{ii}(t)} + \sum_j \frac{(u_j(t))^2}{Q_{jj}(t)} \right\}, \qquad (6)$$

which is dimensionless. The number of elements of the model-data misfit term in equation (6) is the number of the cells ($1^\circ \times 1^\circ \times$ model layer thickness $\times$ 30 days) within which the observations are available (11,700 cells for CFC-11, 11,550 cells for CFC-12).

[37] Observations enter the model at various times and locations, including both the boundaries and model interior. Whenever and wherever an observation that differs from the corresponding model value is available, a forcing term appears in the adjoint model (see W96). The misfit information then propagates as governed by the model dynamics. Observations at or near the open boundaries strongly constrain the open boundary concentrations at the observational locations in the corresponding years, but have little influence on the boundary CFC concentrations at other boundary locations or years, because the yearly mean CFC boundary concentrations are permitted to vary completely independently. In years or places at which there are no observations available at the open boundaries, the corresponding boundary conditions are estimated primarily from information contained in the interior observations. Information flow is such that interior observations carry information only about earlier, not later, boundary conditions (information flow is described more completely by Li and Wunsch, submitted manuscript, 2003).

[38] After 85 iterations, the cost function has been reduced to about 10% of its starting value and is no longer

changing significantly. At that point, the root-mean-square value of the model-data misfit terms in equation (6) is 0.9, near to the desired target of 1, and the computation was halted. On average, the model-data differences fall within the error bars prescribed.

[39] Objective function minimization is achieved primarily by adjustment of the northern boundary concentrations. Adjustment of the piston velocities is negligible, and changes of the initial three-dimensional CFC concentrations are small. Figure 6 shows the unconstrained and constrained CFC-11 distributions at the northern boundary in 1994, a year when comparatively abundant data are available there. Before optimization, there is a large volume of water with CFC-11 concentration about 2.5 pmol/kg located in the deep western basin. This water mass is the CFC-enriched NADW in the unconstrained model. The CFC-11 concentration in the NADW at this location increases from 1 pmol/kg to more than 3 pmol/kg during the interval 1981–1999 before the optimization. Initial estimates of the northern boundary CFC concentrations are too high in the deep western basin, owing to the excessive CFC uptake in high latitudes in the forward model.

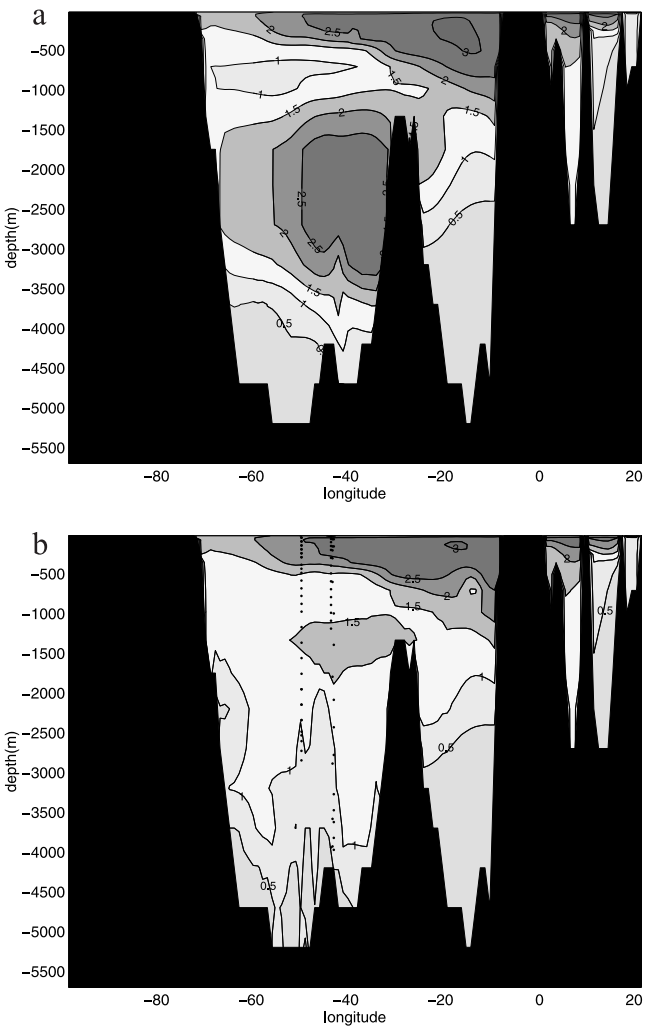

Figure 6. The (top) unconstrained and (bottom) constrained CFC-11 distributions at the northern boundary (39.5°N) in 1994. Units are pmol/kg, and hereafter. In the bottom panel, dots represent observational locations.

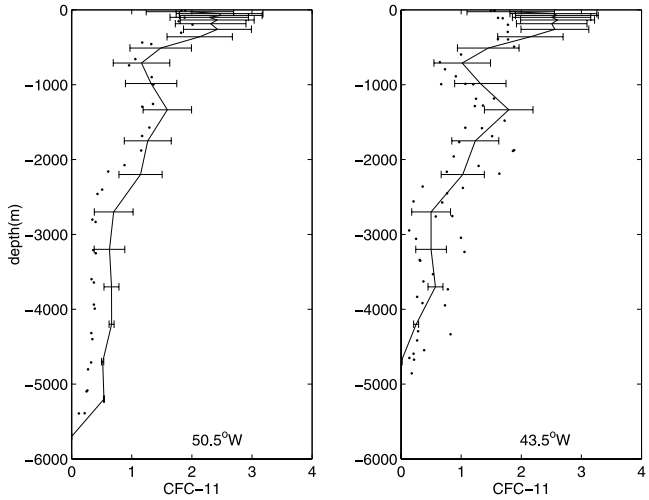

Figure 7. Comparison of the constrained (solid lines) and observational (dots) northern boundary CFC-11 concentrations in 1994. Error bars represent the CFC-11 data error, dominated by the subgrid scale variability the model cannot resolve.

[40] After optimization, the CFC-11 concentration in the western basin between 2000 and 4000 m is greatly reduced (Figure 6). The optimal CFC boundary values at depth are far less than the surface values. Adjustments are large in years and places where observations are available at the open boundary. Adjustments at the boundaries responding to the interior observations are much smaller. In years such as 1994, where deep observations are available at the boundary, the optimized CFC concentrations at the observational locations are reduced strongly, leading to the low CFC values at these locations.

[41] The adjusted boundary values are very close to the observations near there (Figure 7). At 43.5°W, the vertical profile of the observations has some scatter, but the model-data misfits fall within the prescribed error bars. At 50.5°W, the constrained CFC-11 values are similar to those at 43.5°W and are slightly higher than the observations at some depths, because the initial guess was high. We regard this optimal estimate of the boundary values as physically reasonable and as consistent with the present observations and knowledge.

[42] Figure 8 shows the observed and modeled CFC-11 distributions before and after the optimization, along a meridional section 52°W in the western basin where the initial model-data misfit is the largest. Even though the unconstrained model successfully produces some typical features of the observations, as described by *Li* [2003], the modeled CFC-11 concentration in the NADW is far too high. Observed separate deep maxima from two different water sources are not reproduced by the unconstrained model, owing to the problematic model representation of deep water formation in the high latitudes.

[43] The modeled CFC-11 concentration in the NADW has been significantly modified by the optimization. In the constrained model, the CFC-enriched tongue of the upper

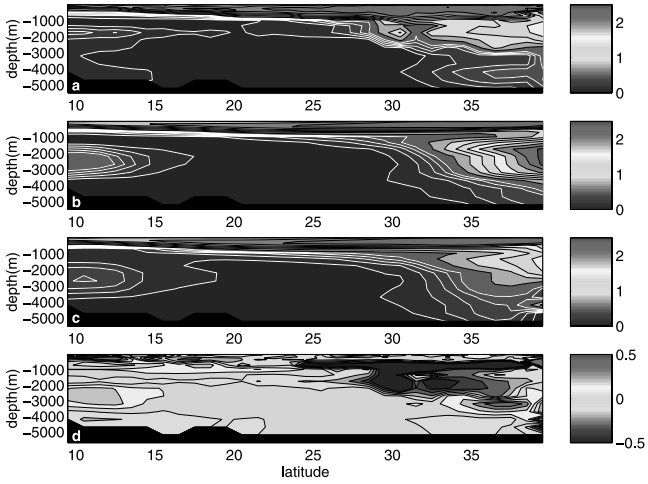

Figure 8. Distributions of (a) observed, (b) unconstrained, (c) constrained, and (d) the differences between the constrained and observed CFC-11 concentrations along ~52°W (WOCE A20), July–August 1997. The contour intervals of white (below 0.5) and black lines (above 0.5) in Figures 8a–8c are 0.1 and 0.25, respectively. The scale of color bar in Figure 8d is different from those in Figures 8a–8c. See color version of this figure at back of this issue.

NADW is rendered more realistically. Both constrained and observed CFC-11 concentrations in the upper NADW have the highest value of 1.5 pmol/kg centered at about 1500 m depth. The tongue of the upper NADW with CFC-11 concentration higher than 0.75 pmol/kg ends at 33°N, in both model and data. At about 4500 m depth, relatively high CFC-11 concentrations appear in the constrained model. The deep maximum at about 4500 m, indicating the signature of the Overflow Water, is visible near the northern boundary. Away from the northern boundary in the model, it is, however, quickly dissipated. This rapid loss is a general feature of a coarse-resolution model [e.g., *England and Holloway*, 1998]. To model the signature of the overflow more realistically, substantially higher horizontal and vertical resolution are required. Nevertheless, by adjusting the boundary conditions alone, the model successfully reproduces the basic large-scale features of the observations.

[44] On average, after optimization, model-data differences fall within the error profiles we have prescribed. Discrepancies however, inevitably exist. Figure 8 also shows the differences between the optimal and observed CFC-11 concentrations along 52°W in the western basin, displaying both negative and positive values. Major differences appear below the ocean surface. Modeled CFC-11 concentrations are too high between 10°N and 15°N at about 300 m depth and too low between 25°N and 39°N at depths 600–900 m. These model-data differences are believed due to the coarse vertical resolution of the model producing too much diffusion [e.g., *Land et al.*, 2001], and the modeled vertical gradient of CFC-11 in the thermocline is too small. At about 33°N, the negative values centered about 2000 m depth are due to the smeared front of Labrador Sea Water in the model, again probably owing to the coarse resolution [e.g., *Redler and Dengg*, 1999]. The

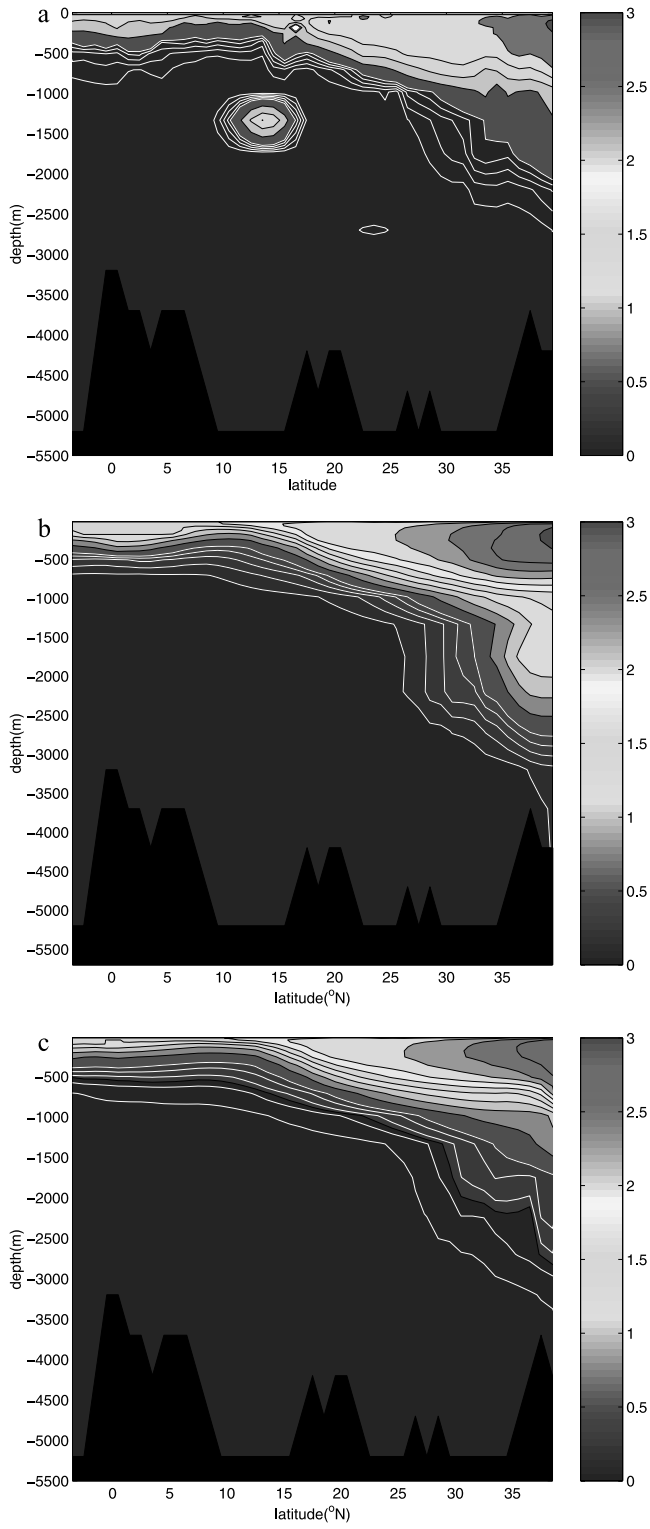

Figure 9. Distributions of (top) observed, (middle) unconstrained, and (bottom) constrained CFC-11 concentrations nominally at 20°W (WOCE AR21, repeated track of Oceanus Cruise 202), July–August 1993. See color version of this figure at back of this issue.

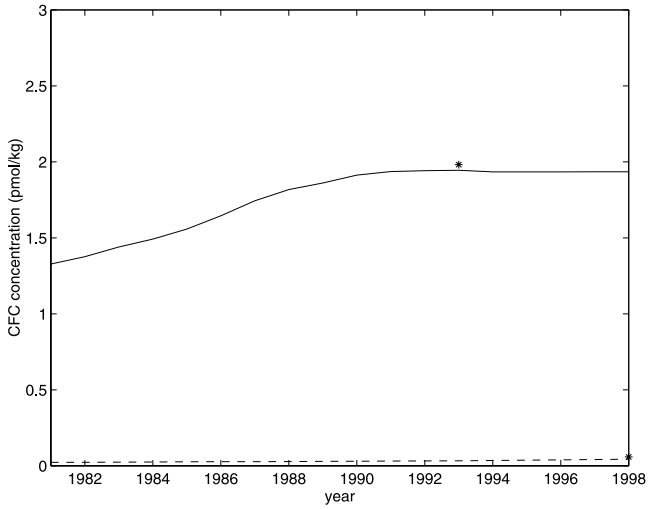

Figure 10. Modeled time series of CFC-11 concentrations at (50.5°W, 24.5°N) at depths 50 m (solid line) and 2200 m (dashed line). The asterisks represent observations.

negative values at about 30°N between 1500 m and 2200 m depth are due to the mesoscale structure that exists in the observations, but is regarded here as data error. At about 3000 m depth, the positive values indicate that modeled CFC-11 concentrations are slightly higher than observations, because the initial estimate is too high. In addition, the steady state simplification of the surface piston velocities and ocean circulation undoubtedly contribute to the model-data misfits to some degree. Nevertheless, at a model resolution of $1° \times 1°$, the model and data are marginally consistent after the optimization of the CFC boundary conditions.

[45] Comparisons of the modeled CFC distributions with observations along other sections show similar characteristics. CFC-11 concentration in the NADW is largely reduced. Modifications of CFC concentrations in the upper ocean and near the bottom, as well as in the eastern basin are relatively small. Figure 9 shows the observed and modeled CFC-11 concentrations nominally along 20°W, July–August 1993, when sufficient CFC has arrived in the deep eastern basin between 30°N and 40°N. Optimization reduces the CFC-11 concentration in the modeled NADW centered at 2000 m depth. After optimization, modeled and observed CFC-11 concentrations at depth are similar: CFC-11 concentration is about 1 pmol/kg at the northern boundary and gradually decreases with depth and latitude; below 2500 m or south of 25°N, the CFC-11 concentration is smaller than 0.1 pmol/kg. In the upper ocean, the large-scale distribution patterns of modeled and observational CFC-11 concentrations agree with each other: high CFC-11 concentration about 2.75 pmol/kg appears at the northern boundary, occupying upper 500 m; the concentration gradually decreases and the CFC isolines shoal toward the surface with latitude. South of 15°N, the CFC content is confined to the near surface. There are, however, obvious model-data differences. Observed mesoscale tracer structure in the upper ocean and near 1500 m are regarded as data error. On the larger scales however, along this section of the eastern basin, the modeled and observed CFC-11 distributions are visually and numerically consistent.

[46] Although there are remaining discrepancies between the optimized fields and the observations, they are generally rationalizable as arising from inadequate model resolution and/or subgrid-scale parameterizations, and not from any fundamental model limitation. The end result here is a (nearly) completely self-consistent representation of the time evolving CFC-11,12 concentrations in three dimensions and time on all grid points represented in the model (e.g., Figure 10), including the time-dependent boundary conditions. We turn now to tritium to examine its use in the same way.

8. Optimization of the Tritium Boundary Conditions

[47] Most tritium entered the ocean in the 1960s via the ocean surface in the high-latitude Northern Hemisphere, where the uptake of surface values is poorly simulated. Not until the 1970s were the earliest measurements of tritium in the ocean made. Radioactive decay into ^{3}He weakens the tritium signals in the deep ocean interior.

[48] Comparisons of the unconstrained model carried to 78.5°N and observed tritium distributions show, as with the CFCs, that the modeled tritium concentration is too high in the high-latitude deep western basin, owing to the too-large vertical penetration in the deep convective regions [*Li*, 2003], and the model domain was again restricted to the region south of 39.5°N.

[49] Tritium observations (Figure 2) in the years 1972–1993 are sparser than those of the CFCs. Because most tritium entered the ocean in the 1960s, an integration period of 1960–1993 is chosen. We again treat the initial and boundary conditions for tritium as control variables. The uncertainty of the temporally and spatially varying tritium surface concentration [see *Li*, 2003] is estimated as 50%, and the relative uncertainties of initial and open boundary tracer concentrations, which come from the forward run, are assumed to be 100%. Whenever the estimated errors are smaller than 0.02 TU, they are re-set to this minimum.

[50] The objective function is formulated in the same way as in equation (6). Yearly-mean surface and open boundary tritium concentrations are prescribed and vary independently each year at each boundary grid in the model. There are 3787 model cells within which the tritium observations are available, a much smaller number than for CFCs.

[51] After 60 iterations, the root-mean-square value of the tritium model-data misfits in equation (6) drops to 1.1 and the computation was stopped. On average, the model-data differences, which are reasonably random in nature, fall within the error-profiles prescribed (these are approximately one-standard errors, and only about 65% of the values should lie within the curves, if the errors are normally distributed).

[52] Figure 11 shows the observed, unconstrained, and constrained tritium distributions along the western Atlantic GEOSECS section, 1972. Before optimization, the tritium-enriched tongue of the NADW is centered at about 2000 m depth in the model, with values too high near the northern boundary. After optimization, the tongue is centered about 1500 m. Constrained tritium concentration in the tongue is

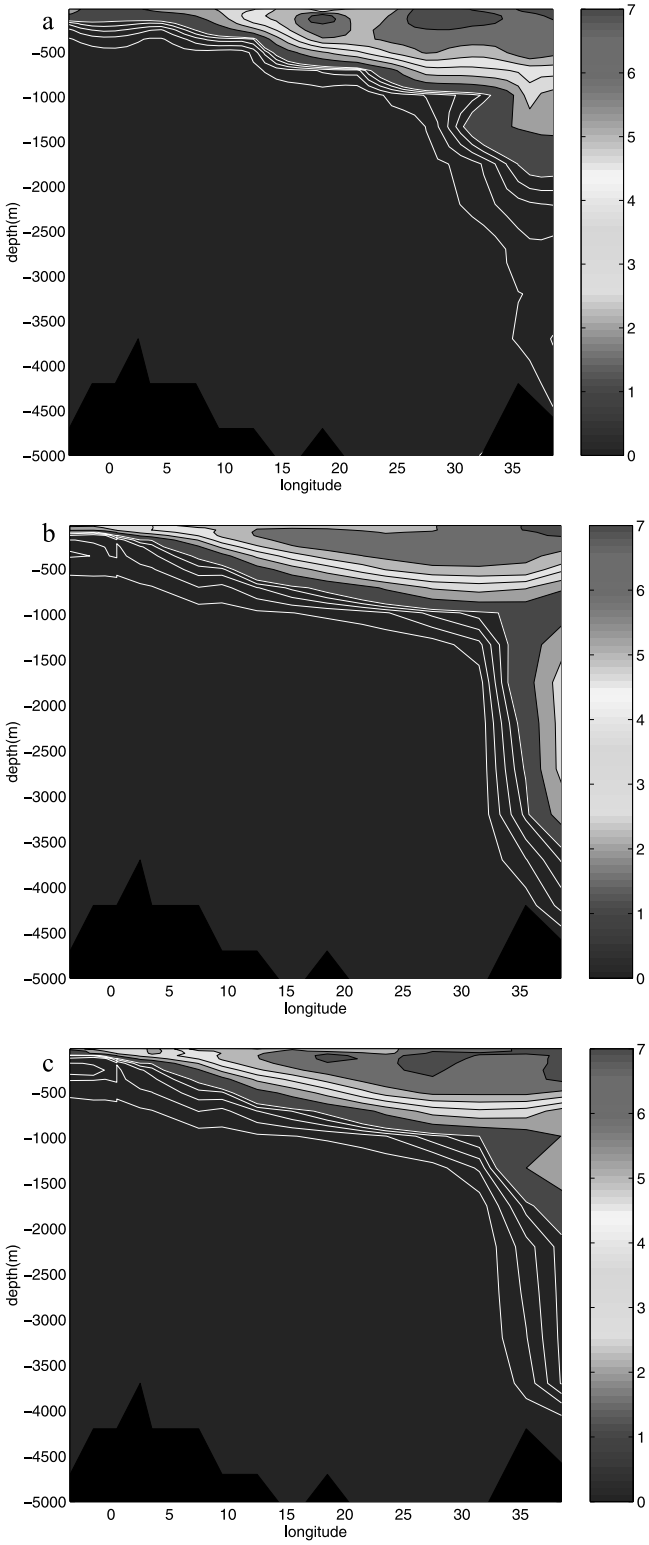

Figure 11. Distributions of (top) observed, (middle) unconstrained, and (bottom) constrained tritium concentrations along the western Atlantic GEOSECS section, 1972. The contour intervals of white (below 1) and black lines (above 1) are 0.2 and 1, respectively. Units are TU and hereafter. See color version of this figure at back of this issue.

similar to the observations; concentrations at 1500 m depth are about 2 TU near the northern boundary, and decrease southward to 1 TU at about 30°N. In the upper ocean, above 500 m, both the constrained and observed tritium distributions show three maxima with values higher than 7 TU

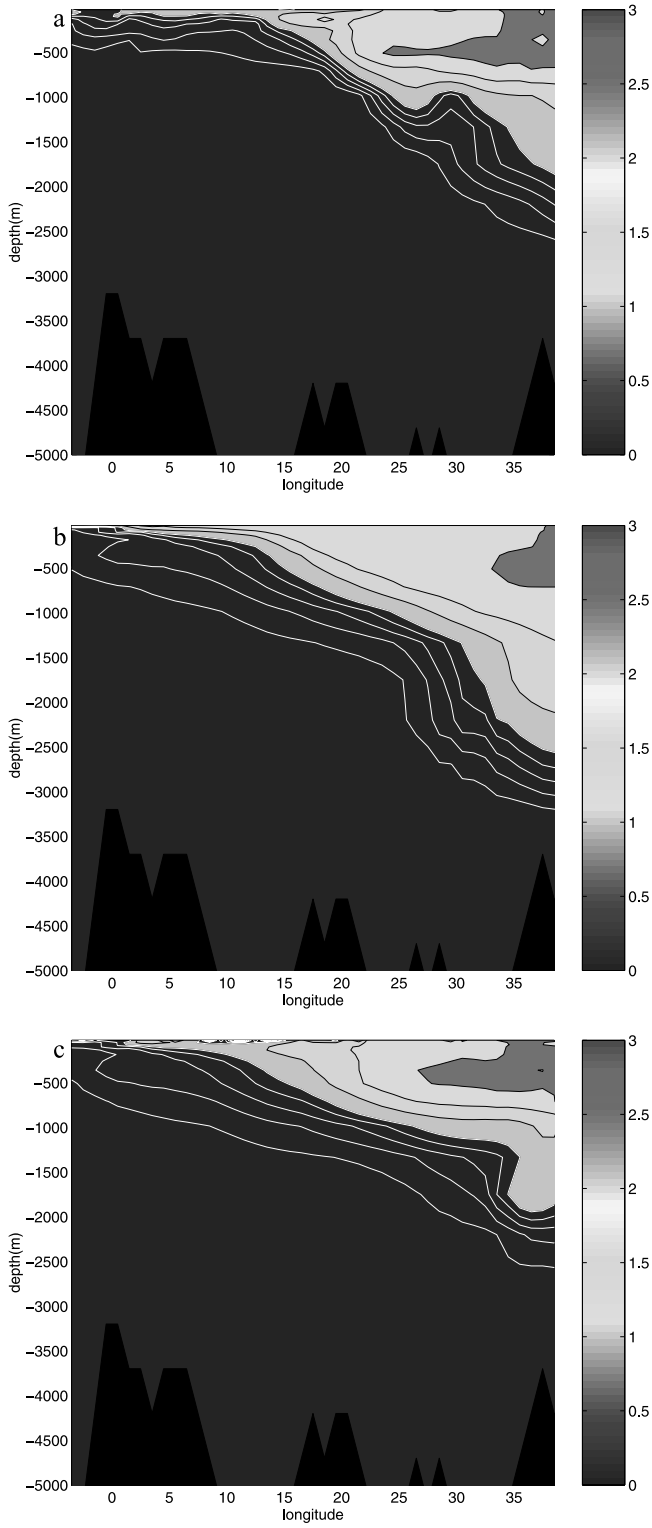

Figure 12. Same as Figure 11, but for the Oceanus Cruise 202 (∼20°W), July–August 1988. See color version of this figure at back of this issue.

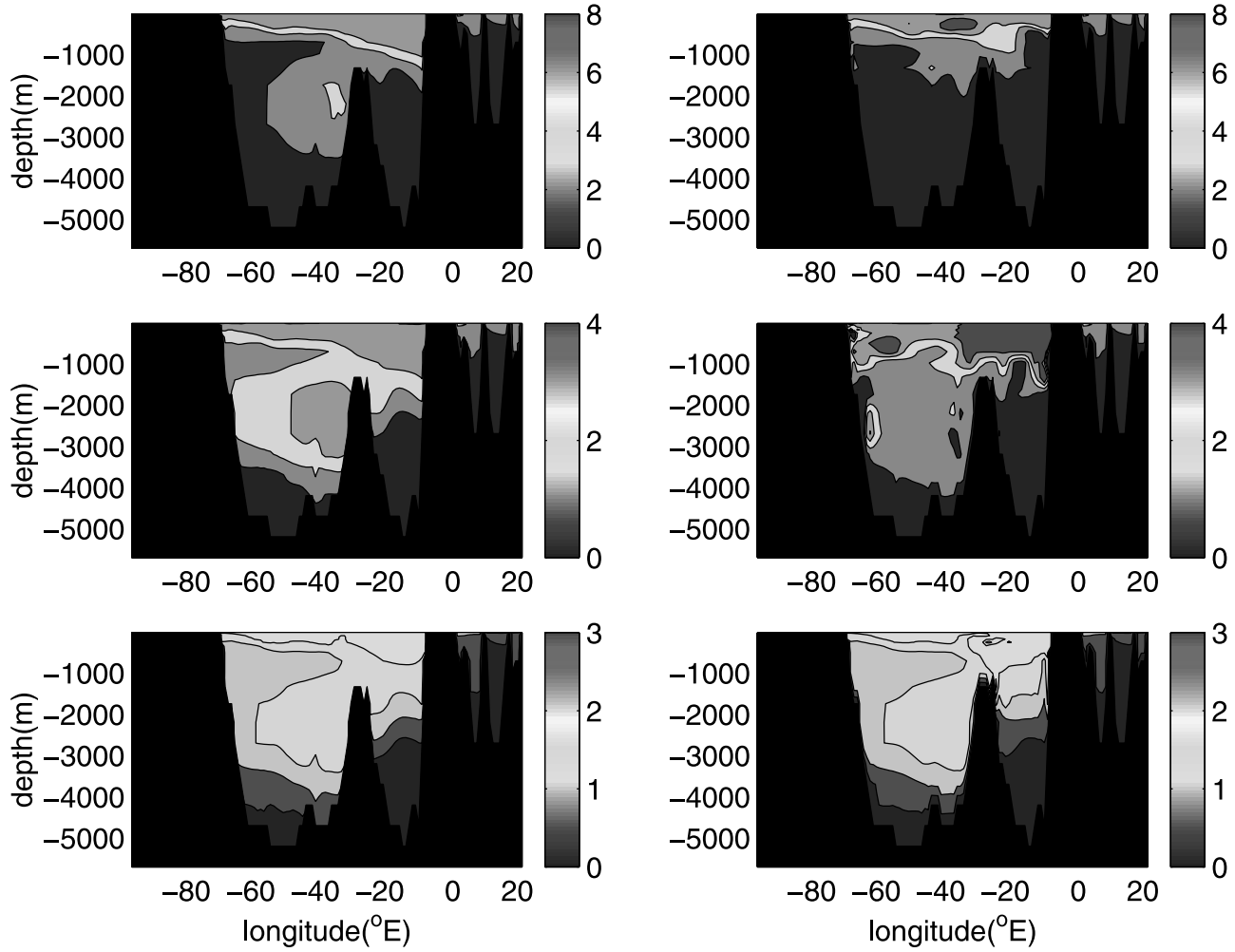

Figure 13. (left) Unconstrained and (right) constrained tritium concentrations at the northern boundary (39.5°N) in (top) 1972, (middle) 1981, and (bottom) 1992. See color version of this figure at back of this issue.

located between 15°N and 20°N, 25°N and 30°N, and near the northern boundary. South of 10°N, most tritium content is confined to the near surface in both constrained model and observations.

[53] The observational, unconstrained, and constrained tritium distributions in the eastern basin, nominally along ∼20°W, July–August 1988, are shown in Figure 12. In the constrained model, the tongue with tritium concentration of 2.5 TU penetrates farther south in the upper ocean, which is more realistic than the unconstrained one. The constrained and observed tritium isolines of 2 TU and 1.5 TU agree with each other. Water with tritium concentration higher than 2 TU penetrates to 20°N and occupies the upper 700 m in both model and data. Near 1500 m, the optimization reduces the modeled tritium concentration. The constrained and observational tritium concentrations below 1000 m are less than 1.5 TU.

[54] As with CFCs, the model-data misfit of tritium is mainly minimized by reducing the modeled tritium concentration in the NADW at the northern boundary. Both the first and optimal estimates of the tritium concentrations at the northern boundary in years 1973, 1981, and 1992, when tritium observations are available, are exhibited in Figure 13. On the largest scale, optimization greatly reduces tritium concentrations between 1500 and 3500 m in the western basin in 1973 and 1981. In 1992, a year before the last available observations, the adjustment of deep tritium concentration at the northern boundary is small. Information about the interior tracer distribution in 1993 carries no information about the northern boundary condition as recent as 1992; the information has not had time to reach that far.

[55] In contrast to the CFCs, where the piston velocity was the control variable, yearly-mean surface tritium values are used. This change greatly increases the number of control variables. Modifications to the first estimates of surface tritium values are larger than those for the CFCs. Adjustments of the surface values in 1981 and 1964 are shown in Figure 14. Large adjustments appear near data locations. Since most tritium entered the ocean in the 1960s, the adjustments of surface values over that period are also obvious. The distribution of the differences in 1964 shows some large-scale features: an increase of surface tritium concentration between 60°W and 40°W near the northern boundary and a decrease in the eastern basin.

[56] The constrained surface tritium values are compared with observations. Figure 15 shows the optimal and

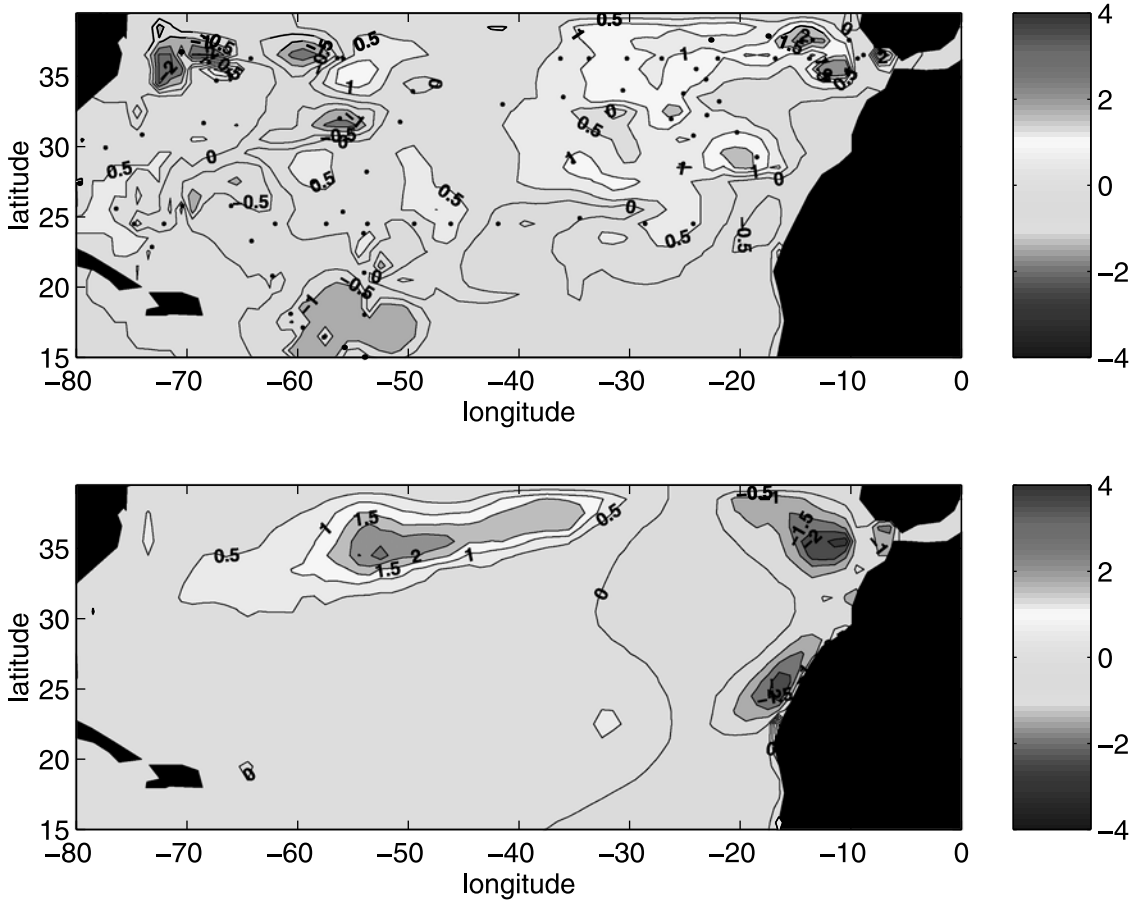

Figure 14. Differences between the constrained and unconstrained (constrained - unconstrained) surface tritium concentrations in (top) 1981 and (bottom) 1964. Black dots in the upper panel represent observational locations. See color version of this figure at back of this issue.

observed tritium distribution in 1981, a year within which there are enough surface tritium observations to form a spatial distribution. The constrained and observational surface tritium concentrations are consistent. Tritium concentration is higher than 4 TU near the northern boundary and in the northeastern basin. Low tritium concentration with values of 2 TU appear in a band from 60°W–70°W, 25°N to 50°W–60°W, 15°N. Tritium concentration in the rest of the model domain is about 3 TU. The optimal boundary conditions, which bring the modeled and observed tracer distributions into consistency, are physically acceptable.

[57] Because there are no tritium observations lying on the model grid at the northern boundary of 39.5°N, comparison of modeled and observational tritium concentrations at the northern boundary is not presented. To obtain some confidence in the estimated tritium boundary conditions, the advective tritium flux across the northern boundary in the constrained model is calculated and compared to an independent estimate [*Doney et al.*, 1993]. Figure 16 shows the cumulative observed tritium input from the ocean surface north of 39.5°N (solid line) from *Doney et al.* [1993] and our estimated southward tritium output across the northern boundary at 39.5°N (dashed line). Most tritium from surface input retains in the ocean north of 39.5°N before 1986, consistent with observations [e.g., *Östlund and Rooth*, 1990; *Doney et al.*, 1993, Figure 4].

[58] Between 4.5°S and 39.5°N, the total oceanic tritium content is obtained from the optimal tritium distribution. Most tritium input into this domain is from the surface and across the northern boundary. Input from the southern boundary is negligible. Surface tritium input flux is taken from *Doney et al.* [1993] rather than from the model, as the tritium concentration boundary condition and poorly resolved mixed layer in the model render the computed surface flux inaccurate. The northern boundary input is obtained from the optimal tritium boundary conditions and the modeled flow field. Figure 17 shows the tritium budget in the region between 4.5°S and 39.5°N. The difference between the total oceanic tritium inventory in the constrained model and the total tritium input from the boundaries is less than 20% in most years, within the uncertainty of the observed surface input. The optimal northern boundary condition of tritium is consistent with the observed tritium budget in the North Atlantic.

9. Discussion and Summary

[59] The use of transient tracers to study the ocean is not straightforward [e.g., *Wunsch*, 2002], and the present results should be regarded primarily as a progress report. Overall, there is no particular difficulty encountered in rendering a constrained GCM consistent with observed transient tracers,

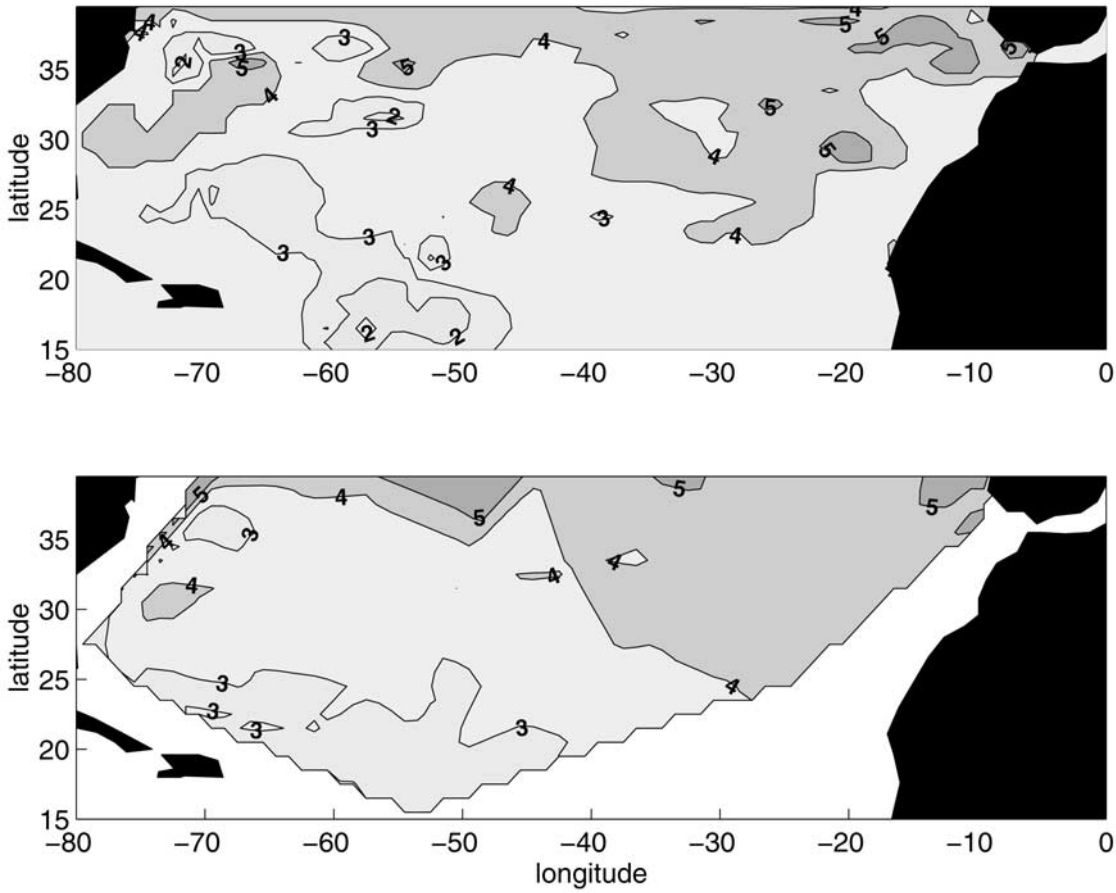

Figure 15. Distributions of the (top) optimal and (bottom) observational surface tritium concentrations in 1981.

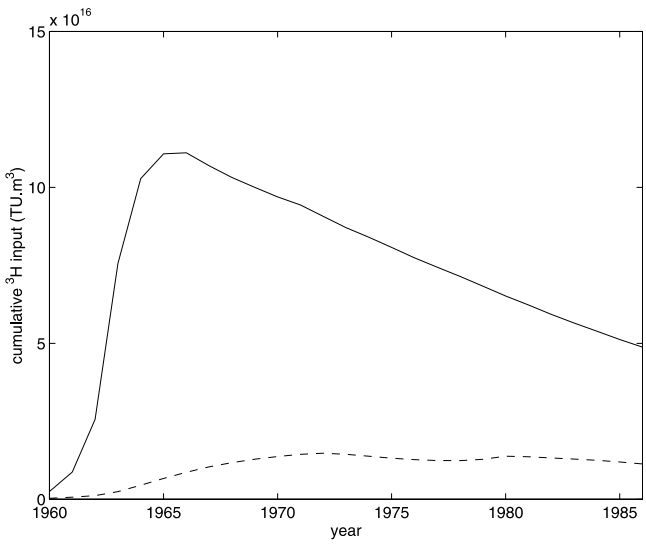

Figure 16. Cumulative observational tritium input from the ocean surface north of 39.5°N (solid line) [*Doney et al.*, 1993] and the constrained southward tritium output across the northern boundary at 39.5°N (dashed line) in the North Atlantic. Note that the radioactive decay of tritium leads to the decrease of values with time.

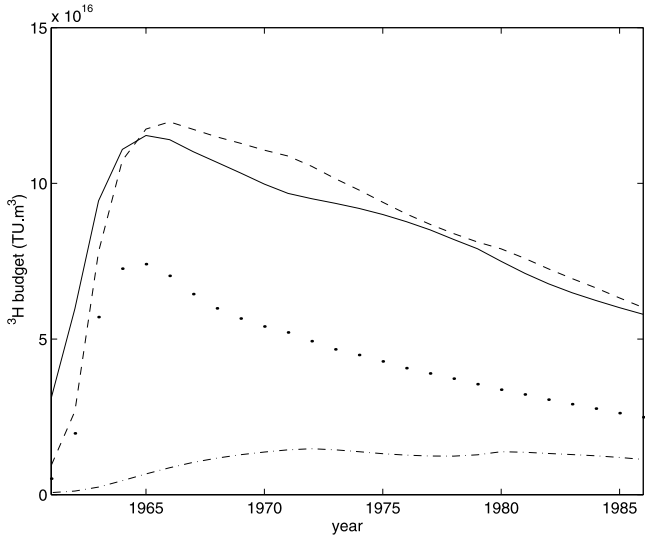

Figure 17. Tritium budget in the region between 4.5°S and 39.5°N in the North Atlantic: solid line, total oceanic tritium content from the constrained model; dashed line, total tritium input from the boundaries; dotted line, cumulative surface input from *Doney et al.* [1993]; dash-dotted line, cumulative northern boundary input in the constrained model.

and the result is a full time-history of tracer content and boundary conditions over the model domain. For example, the net tritium content of this part of the North Atlantic is estimated.

[60] Several limitations to this study exist. In particular, a model with $1^\circ \times 1^\circ$ resolution cannot properly resolve the high-latitude physics, most notably the deep winter convection. (The model inadequacy is, however, already apparent in the temperature and salinity fields.) Experiments, not reported here, to infer improved diffusion coefficients have been successfully carried out. Useful state estimation is here thus limited to non-convective areas, where initial model-data misfits in the upper ocean are comparatively small. As a consequence, the optimizations of both CFC and tritium distributions are mainly controlled by the deep northern boundary conditions. In the non-convective areas, adjustments of the surface CFC values, which are regarded as controlled by the climatological surface piston velocities, are minor. Some obvious adjustments occur in the surface tritium values, which are permitted to vary independently each year. These adjustments, however, are not as strong as those in the northern boundary values.

[61] Owing to the relatively coarse resolution of the model, the tongue of CFC-enriched overflow water in the model is quickly dissipated and is weaker than that in the observations. In the coarse-resolution model, sharp gradients such as the vertical CFC gradients in the thermocline and the front of the CFC-enriched NADW are blurred. These lead to some large-scale model-data differences after optimization. We infer that these would likely disappear if optimization were done at higher resolution.

[62] Other observed transient tracers exist, for example, bomb ^{14}C, that have not been explored in this study. We expect, however, that ^{14}C will exhibit similar characteristics to the CFCs, as both CFCs and ^{14}C enter the ocean through sea surface gas exchange and their atmospheric distributions are quite uniform. It is important to note that this present study focuses on the basin-scale circulation, which is in near-geostrophic balance. Tracer data of any kind is only augmenting information about the circulation largely available from temperature and salinity, data types which are quasi-steady, and available in far greater abundance. It remains possible that transient tracers of the type studied here would have a larger relative information content concerning the much less clearly observed near-surface boundary layer, where geostrophic balance is of little importance. Such a study is beyond our present scope as it requires extremely fine near-surface resolution and higher order dynamics.

[63] State estimation using transient tracer data raises no particular problems not encountered with other types of data used, for example, by *Stammer et al.* [2002], beyond the obvious problems of data coverage of the time evolving fields. By adjusting initial-boundary conditions of CFCs and tritium alone, the $1^\circ \times 1^\circ$ off-line model and the transient tracer data can be brought into near-consistency, in the domain between 4.5°S and 39.5°N of the North Atlantic. Model-data misfits are largely removed by reducing the tracer concentrations in the NADW at the northern boundary.

[64] Because there are now working systems [e.g., *Fukumori et al.*, 1999; *Stammer et al.*, 2002] for rigorous state estimation using full GCMs, the use here of the so-called off-line model, in which the flow field is held fixed, is unnecessary, and the transient tracer data can used to constrain the GCM directly. Because, however, we have found that most of the information in the tracer fields is absorbed in adjusting the boundary-initial conditions, we expect little new information to be available to improve the flow field itself. Li and Wunsch (submitted manuscript, 2003) discuss this issue further.

[65] **Acknowledgments.** This work was supported by NSF award OCE-9730071 (A synthesis of the global WOCE observation), OCE-9617570 (Estimating the climatological annual cycle), and by NASA award NAG5-7857 and NAG5-11933 (A synthesis of the global WOCE observation). We are grateful to all the investigators who allowed us to use their data, either directly or through the WHPO. Thanks are owed in particular to Scott Doney, Thomas Haine, John Bullister, Bill Smethie, Wolfgang Roether, Martin Gould, Laurent Mémery, Peter Schlosser, and Samar Khatiwala. Scott Doney also provided necessary data and associated scripts for computing the CFC age and tritium distributions. The comments of two anonymous referees were helpful. This research has made use of the high performance computational system (Cray Sv1) at the Texas Advanced Computing Center through the National Partnership for Advanced Computational Infrastructure (NPACI).

References

Craig, A. P., J. L. Bullister, D. E. Harrison, R. M. Chervin, and A. J. Semtner Jr., A comparison of temperature, salinity, and chlorofluorocarbon observations with results from a 1 degree resolution three-dimensional global ocean model, *J. Geophys. Res.*, *103*, 1099–1119, 1998.

Deleersnijder, E., J.-M. Campin, and E. J. M. Delhez, The concept of age in marine modelling: I. Theory and preliminary model results, *J. Mar. Syst.*, *28*, 229–267, 2001.

Doney, S. C., and J. L. Bullister, A chlorofluorocarbon section in the eastern North Atlantic, *Deep Sea Res., Part I*, *39*, 1857–1883, 1992.

Doney, S. C., D. M. Glover, and W. J. Jenkins, A model function of the global bomb tritium distribution in precipitation, *J. Geophys. Res.*, *97*, 5481–5492, 1992.

Doney, S. C., W. J. Jenkins, and H. G. Östlund, A tritium budget for the North Atlantic, *J. Geophys. Res.*, *98*, 18,069–18,081, 1993.

Dreisigacker, E., and W. Roether, Tritium and ^{90}Sr in North Atlantic surface water, *Earth Planet. Sci. Lett.*, *38*, 301–312, 1978.

Dutkiewicz, S., M. J. Follows, J. C. Marshall, and W. W. Gregg, Interannual variability of phytoplankton abundance in the North Atlantic, *Deep Sea Res., Part II.*, *48*, 2323–2344, 2001.

England, M. H., and G. Holloway, Simulation of CFC content and water mass age in the deep North Atlantic, *J. Geophys. Res.*, *103*, 15,885–15,901, 1998.

England, M. H., and E. Maier-Reimer, Using chemical tracers to assess ocean models, *Rev. Geophys.*, *39*, 29–70, 2001.

Fukumori, I., R. Raghunath, L.-L. Fu, and Y. Chao, Assimilation of TOPEX/Poseidon altimeter data into a global ocean circulation model: How good are the results?, *J. Geophys. Res.*, *104*, 25,647–25,665, 1999.

Ganachaud, A., and C. Wunsch, Large-scale ocean heat and freshwater transports during the World Ocean Circulation Experiment, *J. Clim.*, *16*, 696–705, 2003.

Gent, P. R., and J. C. McWilliams, Isopycnal mixing in the ocean circulation models, *J. Phys. Oceanogr.*, *20*, 150–155, 1990.

Gent, P. R., J. Willebrand, T. J. McDougall, and J. C. McWilliams, Parameterizing eddy-induced tracer transports in ocean circulation models, *J. Phys. Oceanogr.*, *25*, 463–474, 1995.

Giering, R., and T. Kaminski, Recipes for adjoint code construction, *Trans. Math. Software*, *24*, 437–474, 1998.

Gray, S. L., and T. W. N. Haine, Constraining a North Atlantic ocean general circulation model with chlorofluorocarbon observations, *J. Phys. Oceanogr.*, *31*, 1157–1181, 2001.

Haine, T. W. N., and S. L. Gray, Quantifying mesoscale variability in ocean transient tracer fields, *J. Geophys. Res.*, *106*, 13,861–13,872, 2001.

Haine, T. W. N., and T. M. Hall, A generalized transport theory: Water-mass composition and age, *J. Phys. Oceanogr.*, *32*, 1932–1946, 2002.

Haine, T. W. N., A. J. Watson, M. I. Liddicoat, and R. R. Dickson, The flow of Antarctic Bottom Water to the southwest Indian Ocean estimated using CFCs, *J. Geophys. Res.*, *103*, 27,637–27,653, 1998.

Heinze, C., E. Maier-Reimer, and P. Schlosser, Transient tracers in a global OGCM: Source functions and simulated distributions, *J. Geophys. Res.*, *103*, 15,903–15,922, 1998.

Jenkins, W. J., Determination of isopycnal diffusivity in the Sargasso Sea, *J. Phys. Oceanogr.*, *21*, 1058–1061, 1991.
Kalnay, E., et al., The NMC/NCAR 40-Year Reanalysis Project, *Bull. Am. Meteorol. Soc.*, *77*, 437–471, 1996.
Khatiwala, S., M. Visbeck, and P. Schlosser, Age tracers in an ocean GCM, *Deep Sea Res., Part I*, *48*, 1423–1441, 2001.
Land, C., J. Feichter, and R. Sausen, Impact of the vertical resolution on the transport of passive tracers in the ECHAM4 model, *Rep. 321*, Max-Planck-Insititut für Meteorologie, Hamburg, Germany, 2001.
Ledwell, J. R., A. J. Watson, and C. S. Law, Evidence for slow mixing across the pycnocline from an open-ocean tracer-release experiment, *Nature*, *364*, 701–703, 1993.
Ledwell, J. R., A. J. Watson, and C. S. Law, Mixing of a tracer in the pycnocline, *J. Geophys. Res.*, *103*, 21,499–21,529, 1998.
Li, X., Constraining the North Atlantic circulation with transient tracer observations, Ph.D. thesis, MIT/WHOI Joint Program, Mass. Inst. of Technol., Cambridge, Mass., 2003.
Marotzke, J., R. Giering, K. Zhang, D. Stammer, C. Hill, and T. Lee, Construction of the adjoint MIT Ocean General Circulation Model and application to Atlantic heat transport sensitivity, *J. Geophys. Res.*, *104*, 29,529–29,547, 1999.
Marshall, J., and F. Schott, Open-ocean convection: Observations, theory, and models, *Rev. Geophys.*, *37*, 1–64, 1999.
Marshall, J., C. Hill, L. Perelman, and A. Adcroft, Hydrostatic, quasi-hydrostatic, and nonhydrostatic ocean modeling, *J. Geophys. Res.*, *102*, 5733–5752, 1997a.
Marshall, J., A. Adcroft, C. Hill, L. Perelman, and C. Heisey, A finite-volume, incompressible Navier Stokes model for studies of the ocean parallel computers, *J. Geophys. Res.*, *102*, 5753–5766, 1997b.
Matear, R. J., and C. S. Wong, Estimation of vertical mixing in the upper ocean at station P from chlorofluorocarbons, *J. Mar. Res.*, *55*, 507–521, 1997.
Mémery, L., and C. Wunsch, Constraining the North Atlantic circulation with tritium data, *J. Geophys. Res.*, *95*, 5239–5256, 1990.
Orsi, A. H., G. C. Johnson, and J. L. Bullister, Circulation, mixing, and production of Antarctic Bottom Water, *Prog. Oceanogr.*, *43*, 55–109, 1999.
Östlund, H. G., and G. H. Rooth, The North Atlantic tritium and radiocarbon transients 1972–1983, *J. Geophys. Res.*, *95*, 20,147–20,165, 1990.
Redler, R., and J. Dengg, Spreading of CFCs in numerical models of differing resolution, *Int. WOCE Newsl.*, *35*, 12–14, 1999.
Rhein, M., J. Fischer, W. M. Smethie, D. Smythe-Wright, R. F. Weiss, C. Mertens, D.-H. Min, U. Fleischmann, and A. Putzka, Labrador Sea Water: Pathways, CFC Inventory, and Formation Rates, *J. Phys. Oceanogr.*, *32*, 648–665, 2002.
Schlosser, P., J. L. Bullister, and R. Bayer, Studies of deep water formation and circulation in the Weddell Sea using natural and anthropogenic tracers, *Mar. Chem.*, *35*, 123–136, 1991.
Smethie, W. M., Jr., and R. A. Fine, Rates of North Atlantic Deep Water formation calculated from chlorofluorocarbon inventories, *Deep Sea Res., Part I*, *48*, 189–215, 2001.
Smethie, W. M., Jr., R. A. Fine, A. Putzka, and E. P. Jones, Tracing the flow of North Atlantic Deep Water using chlorofluorocarbons, *J. Geophys. Res.*, *105*, 14,297–14,324, 2000.
Stammer, D., C. Wunsch, R. Giering, C. Eckert, P. Heimbach, J. Marotzke, A. Adcroft, C. N. Hill, and J. Marshall, The global ocean state during 1992–1997, estimated from ocean observations and a General Circulation Model, *J. Geophys. Res.*, *107*(C9), doi:10.1029/2001JC000888, 2002.
Stammer, D., C. Wunsch, R. Giering, C. Eckert, P. Heimbach, J. Marotzke, A. Adcroft, C. N. Hill, and J. Marshall, Volume, heat, and freshwater transports of the global ocean circulation 1993–2000, estimated from a general circulation model constrained by World Ocean Circulation Experiment (WOCE) data, *J. Geophys. Res.*, *108*(C1), 3007, doi:10.1029/2001JC001115, 2003.
Walker, S. J., R. F. Weiss, and P. K. Salameh, Reconstructed histories of the annual mean atmospheric mole fractions for the halocarbons CFC-11, CFC-12, CFC-113 and carbon tetrachloride, *J. Geophys. Res.*, *105*, 14,285–14,296, 2000.
Wanninkhof, R., Relationship between wind speed and gas exchange over the ocean, *J. Geophys. Res.*, *97*, 7373–7382, 1992.
Warner, M. J., and R. F. Weiss, Solubilities of chlorofluorocarbons 11 and 12 in water and seawater, *Deep Sea Res., Part A*, *32*, 1485–1497, 1985.
Waugh, D. W., T. M. Hall, and T. W. N. Haine, Relationships among tracer ages, *J. Geophys. Res.*, *108*(C5), 3138, doi:10.1029/2002JC001325, 2003.
Weiss, W., and W. Roether, The rates of tritium input to the world oceans, *Earth Planet. Sci. Lett.*, *49*, 435–446, 1980.
Wunsch, C., Transient tracers as a problem in control theory, *J. Geophys. Res.*, *93*, 8099–8110, 1988.
Wunsch, C., *The Ocean Circulation Inverse Problem*, Cambridge Univ. Press, New York, 1996.
Wunsch, C., Oceanic age and transient tracers: Analytical and numerical solutions, *J. Geophys. Res.*, *107*(C6), doi:10.1029/2001JC000797, 2002.
Zheng, M., W. J. DeBruyn, and E. S. Saltzman, Measurements of the diffusion coefficients of CFC-11 and CFC-12 in pure water and seawater, *J. Geophys. Res.*, *103*, 1375–1379, 1998.

X. Li, Applied Ocean Physics and Engineering Department, Woods Hole Oceanographic Institution, Woods Hole, MA 02543, USA. (xli@whoi.edu)
C. Wunsch, Department of Earth, Atmospheric and Planetary Sciences, Massachusetts Institute of Technology, Cambridge, MA 02139-4307, USA.

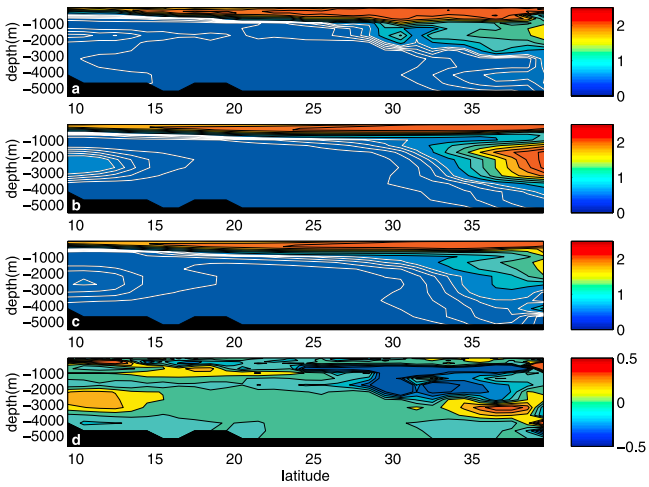

Figure 8. Distributions of (a) observed, (b) unconstrained, (c) constrained, and (d) the differences between the constrained and observed CFC-11 concentrations along ~52°W (WOCE A20), July–August 1997. The contour intervals of white (below 0.5) and black lines (above 0.5) in Figures 8a–8c are 0.1 and 0.25, respectively. The scale ofcolor bar in Figure 8d is different from those in Figures 8a–8c.

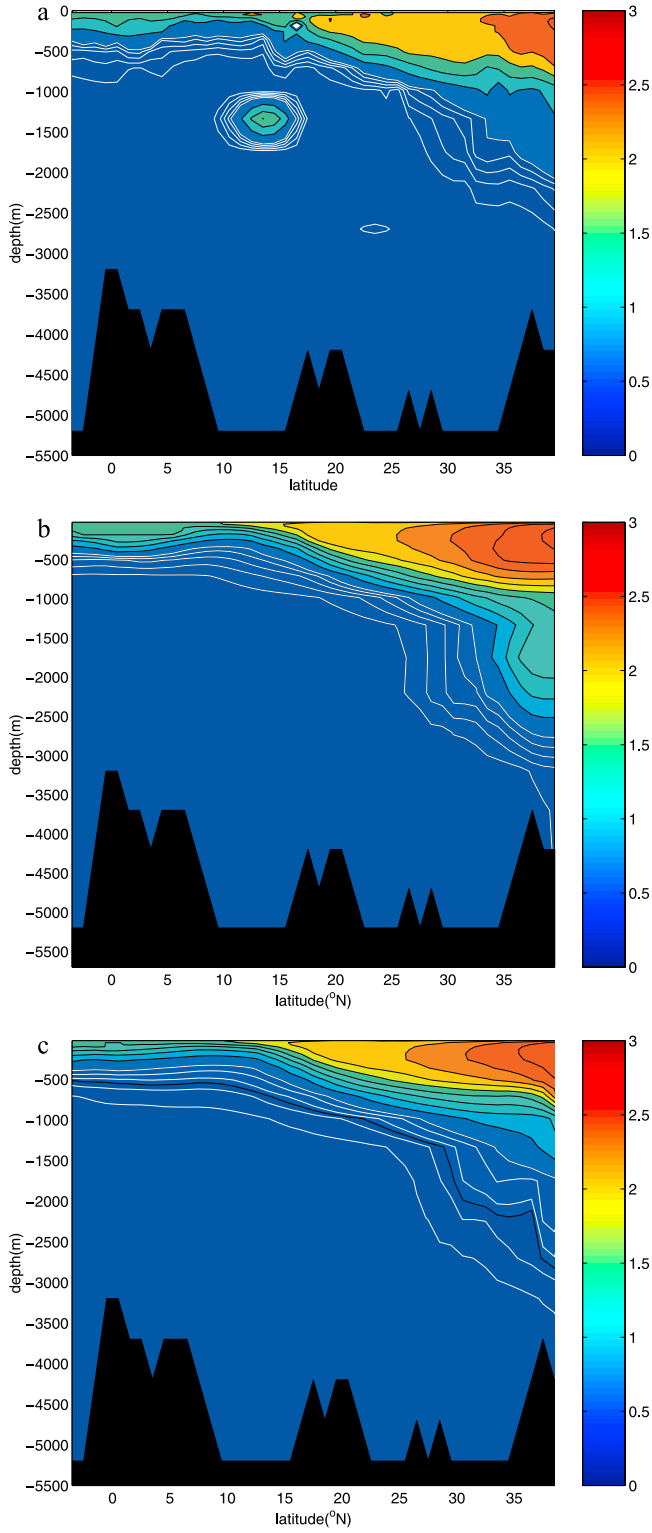

Figure 9. Distributions of (top) observed, (middle) unconstrained, and (bottom) constrained CFC-11 concentrations nominally at 20°W (WOCE AR21, repeated track of Oceanus Cruise 202), July–August 1993.

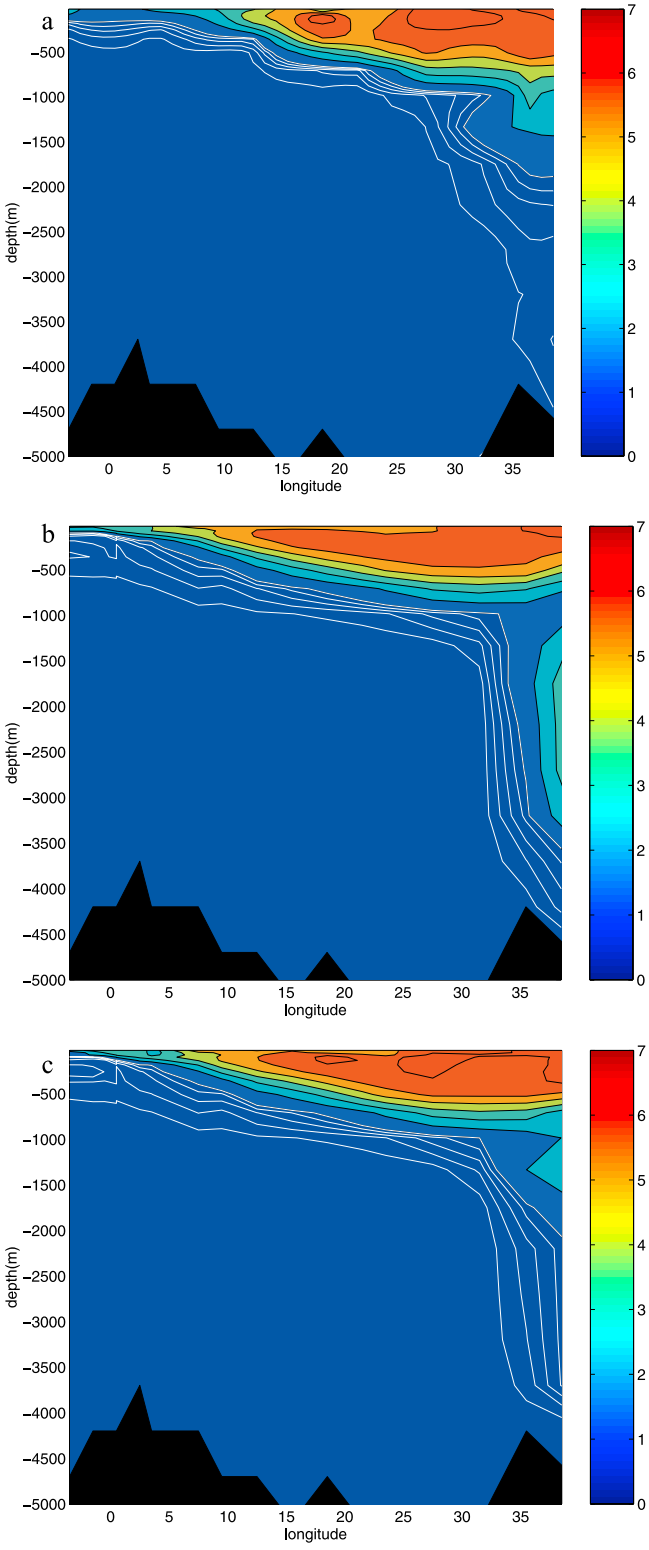

Figure 11. Distributions of (top) observed, (middle) unconstrained, and (bottom) constrained tritium concentrations along the western Atlantic GEOSECS section, 1972. The contour intervals of white (below 1) and black lines (above 1) are 0.2 and 1, respectively. Units are TU and hereafter.

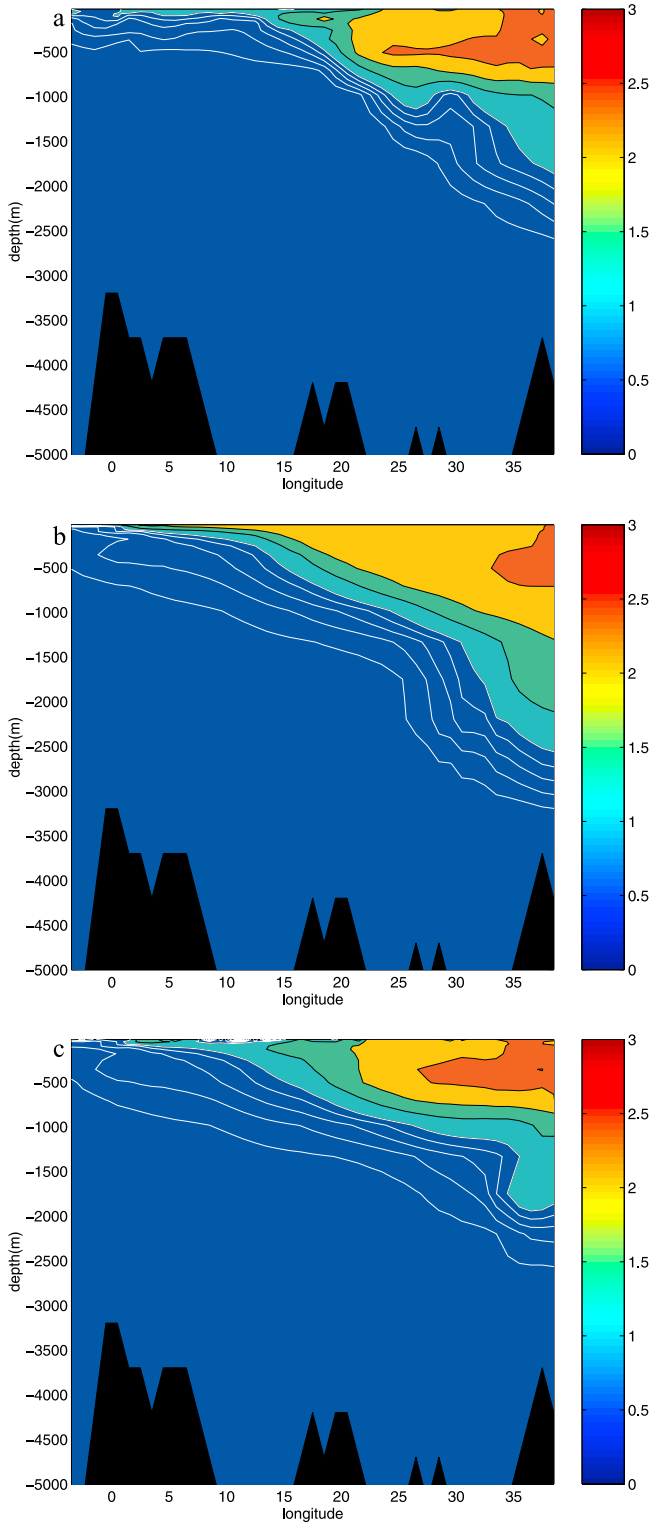

Figure 12. Same as Figure 11, but for the Oceanus Cruise 202 (∼20°W), July–August 1988.

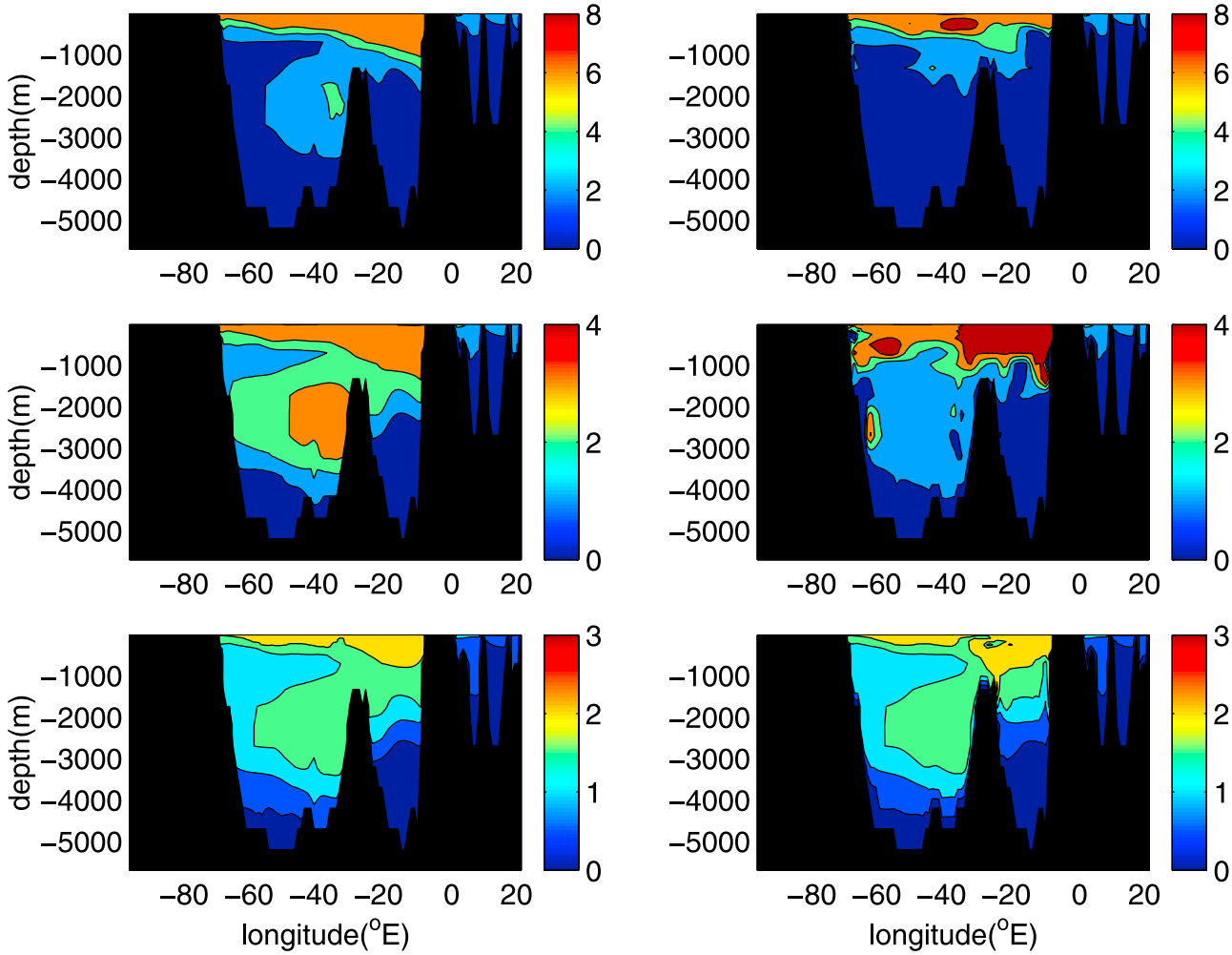

Figure 13. (left) Unconstrained and (right) constrained tritium concentrations at the northern boundary (39.5°N) in (top) 1972, (middle) 1981, and (bottom) 1992.

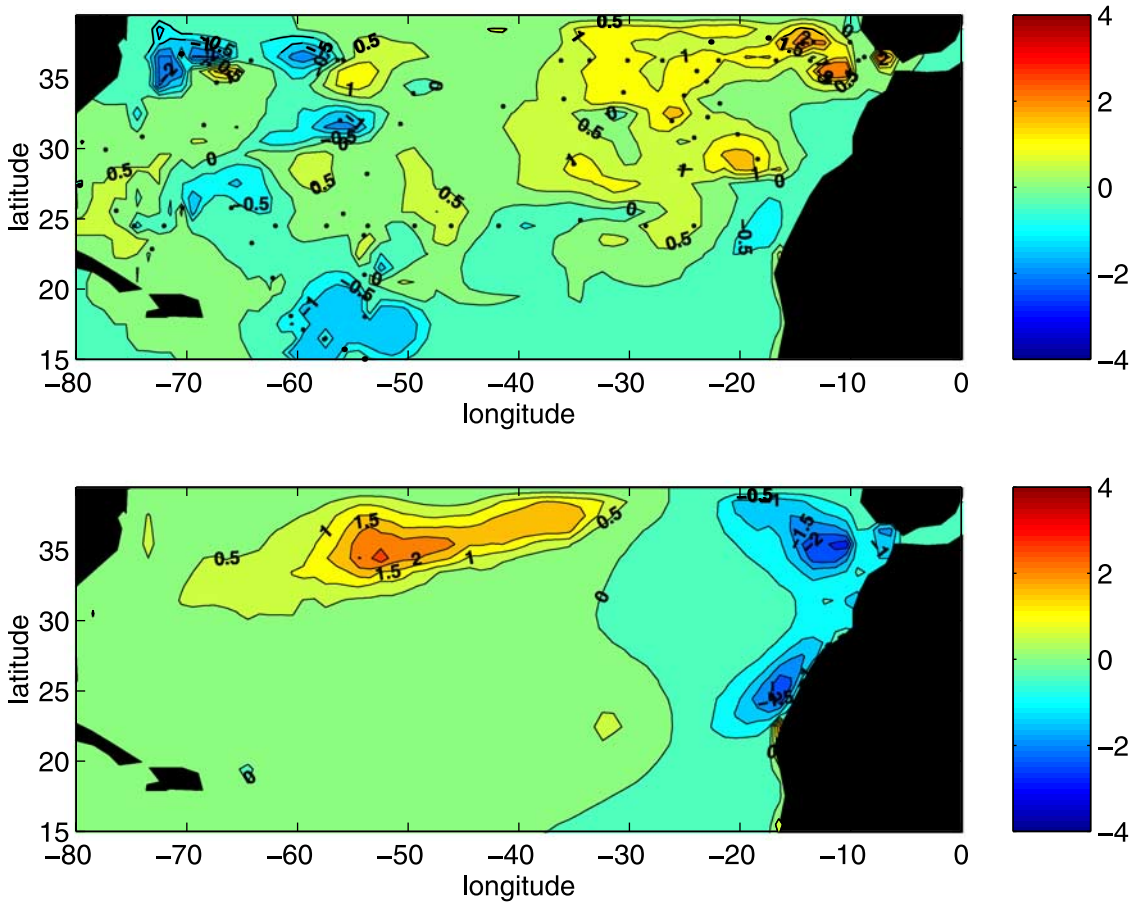

Figure 14. Differences between the constrained and unconstrained (constrained - unconstrained) surface tritium concentrations in (top) 1981 and (bottom) 1964. Black dots in the upper panel represent observational locations.